1970

Mechanical properties and temperature rise in cold hydrostatic extrusion and drawing of ec aluminum

J. E. Oldis
Lehigh University

MECHANICAL PROPERTIES AND TEMPERATURE RISE IN COLD HYDROSTATIC EXTRUSION AND DRAWING OF EC ALUMINUM

J. E. Oldis

ABSTRACT

EC Aluminum was deformed to true strains of approximately 5.8 (reduction in area of 99.7%) both by hydrostatic extrusion and drawing. The as deformed specimens were compared by examining tensile properties, density and grain structure as a function of true strain. Theoretical analysis was employed to estimate back pressure and final aluminum and fluid temperature encountered in hydrostatic extrusion.

The tensile strengths of the extruded specimens increased smoothly to a true strain of approximately 3.0 and then decreased, until, at a true strain of 5.8, they were nearly back to those of the annealed material. This is attributed to recovery and recrystallization as witnessed by metallographic examination. The elongation decreased with true strain and did not increase when the tensile strengths decreased. The tensile strengths of the drawn specimens increased continuously with true strain except for an unexplained discontinuity at a true strain of approximately 3.0.

The density of the hydrostatic extruded specimens increased continuously over the range of true strains measured, while that of the drawn specimens remained essentially unchanged.

The analysis of the aluminum temperature resulted in a final temperature of 555°F for the extruded specimen which showed the inception of recrystallization. The aluminum temperature and extrusion back pressure are probably somewhat lower than actual, since the

analysis did not include the effect of strain rate on the flow stress of the material and are therefore affected little by changes in final velocity. The analysis showed that the temperature rise of the fluid is small, and is affected by changes in true strain, final velocity and die cone angle.

MECHANICAL PROPERTIES AND TEMPERATURE RISE IN COLD HYDROSTATIC EXTRUSION AND DRAWING OF EC ALUMINUM

by

J. E. Oldis

A THESIS

Presented to the Graduate Faculty

of Lehigh University

in Candidacy for the Degree of

Master of Science

in

Metallurgy and Materials Science

Lehigh University
1970

COMPANY PRIVATE

TECHNICAL REPORT COVER SHEET

TITLE: Mechanical Properties and Temperature Rise In Cold Hydrostatic Extrusion and Drawing of EC Aluminum

AUTHOR(S): J. E. Oldis

DEPARTMENT: 31PRZ13421
LOCATION: Princeton
LOCAL REPORT NUMBER: CC 4010
DATE: June 2, 1970

Case No. 15027

ABSTRACT: EC Aluminum was deformed to true strains of approximately 5.8 (reduction in area of 99.7%) both by hydrostatic extrusion and drawing. The as deformed specimens were compared by examining tensile properties, density and grain structure as a function of true strain. Theoretical analysis was employed to estimate back pressure and final aluminum and fluid temperature encountered in hydrostatic extrusion.

The tensile strengths of the extruded specimens increased smoothly to a true strain of approximately 3.0 and then decreased, until, at a true strain of 5.8, they were nearly back to those of the annealed material. This is attributed to recovery and recrystallization as witnessed by metallographic examination. The elongation decreased with true strain and did not increase when the tensile strengths decreased. The tensile strengths of the drawn specimens increased continuously with true strain except for an unexplained discontinuity at a true strain of approximately 3.0. (Abstract cont. on next page)

REFERENCES:

INDEXING TERMS: EC Aluminum, Hydrostatic Extrusion, Drawing, Mechanical Properties, Temperature Rise

---

Have you sent a copy of this report to your Patent Organization? Yes X No ____

Should the distribution of your report be restricted? Yes ____ No X

J. W. Archer

APPROVAL

The Patent Organization may not have made a complete investigation of the patent aspects of the information disclosed in this Technical Report. Therefore, anyone wishing to introduce into Western's commercial products or operations any process, apparatus, equipment, material or tool mentioned herein should consult the Patent Attorney functional for his location before taking any definite action in that direction.

Send reproducible copy of cover sheet and report to:

INFORMATION SCIENCE DEPARTMENT
Engineering Research Center
Western Electric Company, Inc.
P. O. Box 900
Princeton, New Jersey 08540

The density of the hydrostatic extruded specimens increased continuously over the range of true strains measured, while that of the drawn specimens remained essentially unchanged.

The analysis of the aluminum temperature resulted in a final temperature of 555°F for the extruded specimen which showed the inception of recrystallization. The aluminum temperature and extrusion back pressure are probably somewhat lower than actual, since the analysis did not include the effect of strain rate on the flow stress of the material and are therefore affected little by changes in final velocity. The analysis showed that the temperature rise of the fluid is small, and is affected by changes in true strain, final velocity and die cone angle.

CERTIFICATE OF APPROVAL

This thesis is accepted and approved in partial fulfillment of the requirements for the degree of Master of Science.

May 13, 1970
(Date)

Professor in Charge

Chairman of the Department
of Metallurgy and Materials Science

ACKNOWLEDGMENTS

The author wishes to thank Dr. Betzalel Avitzur of the Lehigh University Metallurgy and Materials Science Department and Messrs. F. J. Fuchs and J. W. Archer of Western Electric Company for their guidance and helpful suggestions throughout the course of this investigation, which was made possible by the Lehigh University-Western Electric Company Fellowship Program. Thanks are also extended to Messrs. N. Ahmed, J. S. Cartwright, G. L. Schmehl and S. J. Buzash for their assistance. Typing was performed cheerfully and conscientiously by Miss Elaine Yesco and Mrs. Robyn Trus to whom the author is grateful. In addition, many others provided useful information and cooperation, all of which is sincerely appreciated.

TABLE OF CONTENTS

		Page
	ABSTRACT	1
I.	INTRODUCTION	3
II.	EXPERIMENTAL PROCEDURES	6
	A. Specimen Preparation	6
	B. Hydrostatic Extrusion Equipment and Production	6
	C. Drawing Equipment and Production	9
	D. Specimen Studies	10
	1. Tensile Tests	10
	2. Density Measurements	12
	3. Metallography	14
III.	RESULTS AND DISCUSSION	16
	A. Mechanical Properties	16
	B. Extrusion Pressure and Die Angle	19
	C. Density	21
	D. Photomicrographs	22
	E. Theoretical Consideration of Temperature Rise	23
IV.	CONCLUSIONS AND RECOMMENDATIONS	32
	FIGURES	34
	TABLES	64
	APPENDIX I	80
	BIBLIOGRAPHY	85
	VITA	89

LIST OF FIGURES

Figure		Page
1	Pressure Vessel and Press	34
1.5	Typical Pressure Versus Time Recording	36
2	Density Versus Temperature	37
3	Extended True Stress Versus True Strain	38
4	Extended True Stress Versus True Strain	39
5	Extended True Stress Versus True Strain	40
6	Extended True Stress Versus True Strain	41
7	Elongation Versus True Strain	42
8	Elongation Versus True Strain	43
9	True Strain Versus Average Extrusion Runout Pressure	44
10	Effect of Cone Angle on Wire Surface	45
11	True Strain Versus Average Relative Density	46
12	500X Photomicrographs E C Aluminum	47
13	Die and Extrusion Geometry	48
13.5	Increase in Flow Stress Through Die	49
14	Extrusion Back Pressure Versus True Strain	50
15	Effect of True Strain on Optimum Die Angle	51
16	Aluminum Final Temperature Versus True Strain	52
17	Fluid Final Temperature Versus True Strain	53
18	Effect of True Strain on $\frac{\varepsilon}{R_f}$	54
19	Extrusion Back Pressure Versus Semicone Angle	55
20	Aluminum Final Temperature Versus Semicone Angle	56

Figure		Page
21	Effect of Semicone Angle on Fluid Temperature	57
22	Effect of Semicone Angle on $\frac{\varepsilon}{R_f}$	58
23	Effect of Velocity on Optimum Cone Angle	59
24	Extrusion Back Pressure Versus Final Velocity	60
25	Aluminum Final Temperature Versus Final Velocity	61
26	Fluid Final Temperature Versus Final Velocity	62
27	Effect of Final Velocity on $\frac{\varepsilon}{R_f}$	63

LIST OF TABLES

Table		Page
1	Hydrostatic Extrusion Tensile Properties E C Aluminum	64
2	Average Runout Pressure and Velocities Hydrostatic Extruded E C Aluminum	68
3	Drawn Tensile Properties E C Aluminum	69
4	Annealed Tensile Properties E C Aluminum	73
5	Density Data Diethylene Glycol Monoethyl Ether	74
6	Density Data - 22 °C Hydrostatic Extruded E C Aluminum	75
7	Density Data - 22 °C Drawn E C Aluminum	77
8	Average Relative Density E C Aluminum	79

ABSTRACT

EC Aluminum was deformed to true strains of approximately 5.8 (reduction in area of 99.7%) both by hydrostatic extrusion and drawing. The as deformed specimens were compared by examining tensile properties, density and grain structure as a function of true strain. Theoretical analysis was employed to estimate back pressure and final aluminum and fluid temperature encountered in hydrostatic extrusion.

The tensile strengths of the extruded specimens increased smoothly to a true strain of approximately 3.0 and then decreased, until, at a true strain of 5.8, they were nearly back to those of the annealed material. This is attributed to recovery and recrystallization as witnessed by metallographic examination. The elongation decreased with true strain and did not increase when the tensile strengths decreased. The tensile strengths of the drawn specimens increased continuously with true strain except for an unexplained discontinuity at a true strain of approximately 3.0.

The density of the hydrostatic extruded specimens increased continuously over the range of true strains measured, while that of the drawn specimens remained essentially unchanged.

The analysis of the aluminum temperature resulted in a final temperature of 555°F for the extruded specimen which showed the inception of recrystallization. The aluminum temperature and extrusion back pressure are probably somewhat lower than actual, since the

analysis did not include the effect of strain rate on the flow stress of the material and are therefore affected little by changes in final velocity. The analysis showed that the temperature rise of the fluid is small, and is affected by changes in true strain, final velocity and die cone angle.

I. INTRODUCTION

The judicious application of pressure has been used in metal forming for many centuries. In the ancient process of wire drawing the pressures exerted by the die permit much greater extension than can be achieved by simple tension, although a good understanding of the contributions of the various components of stress has been developed primarily in this century.

Von Mises[1] considered the stress deviator components to influence yielding and this theory is still generally accepted, except perhaps at extremely high hydrostatic stress levels, which cause an increase in the yield stress of the material[2]. The experiments of Bridgman[3,4] showed that the hydrostatic stress component has a profound effect on the ductility of metals. It is generally accepted that the increase in ductility caused by increasing the hydrostatic stress component is due to the suppression of pore and void formation during plastic deformation[5,6,7].

In recent years intensive efforts have been made by many investigators[8,9,10] in an effort to utilize this hydrostatic pressure induced increase in ductility to obtain greater deformation of ductile materials and any deformation at all with brittle materials. One of the areas under current investigation is the production of electrical conductors by hydrostatic extrusion. Because of the large fluctuations in the price of copper, increasing attention is being given to the use of aluminum as a conductor material. Because it is important to know the effect of the production process variables

on the as-formed properties of the material, this study was initiated to compare the properties of conventionally drawn electrical conductor (EC) aluminum with those hydrostatically extruded with atmospheric front pressure. The properties investigated here are the bulk mechanical properties as obtained by tensile testing, the changes in density with true strain as obtained by a differential weighing technique, and the changes in structure with true strain as observed with photomicrographs.

Fully annealed commercially available EC-aluminum (99.45% al) was used for all specimens. Approximately eighty hydrostatic extrusions were produced at true strains (ϕ) up to 5.87 where:

$$\phi = 2\ln \frac{D_o}{D_f} \qquad (1)$$

and D_o = Initial Diameter

D_f = Final Diameter

These were made using a multiwall pressure chamber, fitted with dies of several cone angles, seals and piston, in a 200 ton hydraulic press. Drawing was done in increments of approximately 20% reduction in area for the same range of true strains (ϕ). Dies having semicone angles of $\alpha = 8^\circ$ were used and the drawing force was provided by an overhead crane. Tensile tests were made in an Instron testing machine using a ten inch gage length for all tests. Approximately 60 extrusions and 60 drawn samples were tested. Density measurements were obtained using a differential weighing technique on a single pan microgram balance. Approximately 24 series of weighings

were made. Photomicrographs were prepared using standard mounting, polishing and etching techniques.

A detailed description of the procedures used in this investigation is presented in the following section. The third section will analyze and interpret the data obtained and will also present an analysis of the temperature rise encountered in hydrostatic extrusion. The conclusions and recommendations resulting from the study are presented in section four. Appendix I will present background information on material properties as affected by hydrostatic processes as reported in the literature.

II. EXPERIMENTAL PROCEDURES

This section of the report will present the methods of specimen preparation, extrusion equipment and production, and the techniques and equipment employed in producing drawn specimens. The procedures used in studying the as extruded and as drawn specimens, i.e., mechanical testing, density measurements and metallographic examination are also outlined.

A. Specimen Preparation

All specimens used in this study were prepared from the same section of a coil of 7/16 inch diameter ECH-12 aluminum (99.45 + % al) redraw rod produced from scalped ingots. Specimens were prepared by drawing the rod to .406 inch diameter, straightening, and redrawing to .3652 inch diameter, the initial diameter (D_o) of all extruded and drawn specimens in this study. The billets to be used for extrusion were then machined to ten inch lengths, which was adequate to provide the volume of material required for ten inch gage lengths for tensile testing at all reductions. One end of these billets was pointed with a semicone angle 2 1/2° to 5° less than the semicone angle (α) of the die through which it would be extruded. Adequate lengths of billet were provided so that ten inch gage lengths of drawn material could be obtained at the reductions desired. All billets were then annealed at 650°F for one hour and cooled in air.

B. Hydrostatic Extrusion Equipment and Production

All extrusions were performed using a composite Vascomax 300*

*Vanadium Alloys Steel Co., Latrobe, Penna.

chamber capable of withstanding approximately 150,000 psi, in conjunction with a 200 ton hydraulic press, as shown in Figure 1. The press and the two wall pressure chamber were existing equipment at the Western Electric Company Engineering Research Center, Princeton, N. J. The pistons, dies, inner liner, removeable liner, downstops, piston retainer and bearing plate were designed and constructed from Vascomax 300, heat treated at 900°F for three hours and air cooled. Buna N "O" rings and Beryllium Copper anti-extrusion rings were used as inter-changeable seals on the pistons and dies.

The chamber was loaded by inserting the billet into the removeable liner (approximately .005 inch radial clearance between billet and liner) with the tapered nose of the billet pressed firmly into the die. The remaining volume of the chamber was then filled with Cindol 4683* and some time allowed for any entrapped air to escape. The ram was then lowered and the extrusion made. The downstop was adjusted prior to extrusion so that the extruded rod did not contact the press platen. Ten inch billets and low billet velocity (v_o = .17 in/sec) were used for all extrusions up to a true strain (ϕ) of 2.31. For extrusions to true strains (ϕ) greater than 3.0 the billet length was reduced to two inches and the billet velocity (v_o) was increased to .84 in/sec at true strains (ϕ) of approximately 4.0 and to 1.41 in/sec at true strains (ϕ) of approximately 5.9. In the case of the two

*E. F. Houghton & Company, Phila., Penna.

largest true strains, $\phi \approx 4$ and $\phi \approx 5.9$, no downstop was used and the extruded wire coiled (coil diameter approximately 14 inches) within the confines of the standoffs (see Figure 1).

True strain (ϕ) as used in this study has been defined as:

$$\phi = 2\ln \frac{D_o}{D_f} \tag{1}$$

which is the ideal effective strain and assumes no distortion. A more precise expression for the strain induced in the product would incorporate the effects of redundant and frictional deformation. Avitzur's[11] equation (8.63) suggests that a more realistic expression would be:

$$\phi = 2f(\alpha)\ln \frac{D_o}{D_f} + \frac{2}{\sqrt{3}}\left(\frac{\alpha}{\sin^2\alpha} - \cot\alpha\right) \tag{1.1}$$

$$\text{where, } f(\alpha) = \frac{1}{\sin^2\alpha}\left[1 - (\cos\alpha)\sqrt{1 - \frac{11}{12}\sin^2\alpha} + \frac{1}{\sqrt{11\cdot 12}} \cdot \ln \frac{1 + \sqrt{\frac{11}{12}}}{\sqrt{\frac{11}{12}}\cos\alpha + \sqrt{1 - \frac{11}{12}\sin^2\alpha}}\right] \tag{1.2}$$

This incorporates redundant deformation but not frictional deformation. For the small cone angles used in this study ($\alpha \leq 30°$), f (α) is close to one and $\frac{2}{\sqrt{3}}\left(\frac{\alpha}{\sin^2\alpha} - \cot\alpha\right)$ has a relatively small effect at large reductions. Equation (1) is therefore used as the basis of comparison. It can also be seen that discrepancies will arise when comparing drawn and extruded products using equation (1), due to the difference in the schedules of reduction per pass and die angles used.

Pressure versus time recordings were made for each extrusion on a Brush recorder, using the pressure behind the press piston. This pressure is undoubtedly different from that present in the extrusion chamber, but is nevertheless used as the extrusion pressure (after adjustment with the proper area ratio). Figure 1.5 shows a typical recording and defines the average runout pressure. The velocity of the billet (v_o) was obtained by taking the length of the billet extruded and dividing by the time observed on the recording. The final velocity (v_f) of the wire was obtained from $v_f = v_o\left(\frac{D_o}{D_f}\right)^2$, which is based on the assumption of a constant volume process. Tables 1 through 4 present the details of the specimens produced for subsequent testing. Table 1 shows the schedule of semicone angles (α) and true strains (ϕ) used in hydrostatic extrusion and Table 2 shows the average runout pressures (P_b), initial velocity (v_o), and final velocity (v_f) at each reduction.

C. Drawing Equipment and Production

Specimens were drawn through dies having semicone angles (α) of 8° at a reduction in area of approximately 20 percent per die. Carbide dies were used for sizes greater than .080 inch diameter and diamond dies for .080 inch diameter and less. An overhead crane provided the drawing force and Cindol 4683 was used as the lubricant. A constant wire final velocity (v_f) of approximately 3.1 in/sec was used for all passes. Table 3 shows the schedule

of true strains (ϕ) obtained for subsequent testing.

D. Specimen Studies

1. Tensile Tests

Approximately 60 extrusions and 60 drawn wires were tested, in addition to tests on the annealed, undeformed aluminum from which all extrusions and drawings were made. Tests were made on an Instron testing machine which provided the load-displacement data from which true stress-true strain data was obtained. Table 1, 3 and 4 show the true strains obtained by prior deformation at which these tests were made. From two to seven tests were made on each reduction deformed by a given process. The tests were made on the products in the exact form as they emerged from the dies, since the properties of the whole wire were of interest. Because of the lack of a well defined gage length, some problems were encountered in necking in or near the grips and when this occurred the test was discarded. A ten inch gage length (ten inches between grip faces) was used for all diameters, although elongation at fracture measurements made in this manner are not directly comparable[12]. To compare elongation at fracture measurements, the specimens must be geometrically similar, i.e., the ratio of gage length to diameter must be constant so that the influence of localized deformation at the neck on the total elongation of the gage length remains constant. Elongation

at ultimate load is not affected by geometry since prior to this point necking has not occurred and the specimen elongates and contracts in diameter uniformly. A crosshead speed of 0.1 inch/minute was utilized resulting in a strain rate of .01/minute. This strain rate was not constant throughout a given test however, since as elongation increased the strain rate decreased.

The load-displacement data from the Instron recording was converted to true stress-true strain data as follows:

a. .2% Offset True Yield Stress ($\sigma_{.002}$)

$$\sigma_{.002} = S_{.002} (1 + \varepsilon_{.002}) \qquad (2)$$

where, $S_{.002}$ = Engineering Stress = $\frac{P_R}{A_o}$ (lbs/in^2)

P_R = Instantaneous Load (lbs)

A_o = Original Area (in^2)

$\varepsilon_{.002}$ = Engineering Strain = $\varepsilon_1 + \varepsilon_2$ (in/in)

$\varepsilon_1 = \frac{\Delta l}{l_o} = \frac{.002 \times 10 \text{ in}}{10 \text{ in}} = .002$ (in/in)

$\varepsilon_2 = \frac{S_{.002}}{E}$ (in/in)

E = Elastic Modulus = 10×10^6 (lbs/in^2)

b. .2% Offset True Yield Strain ($\phi_{.002}$)

$$\phi_{.002} = \ln (1 + \varepsilon_{.002}) \qquad (3)$$

where, $\varepsilon_{.002}$, ε_1, and ε_2 as defined above

c. True Stress at Ultimate Load (σ_{ult})

$$\sigma_{ult} = S_{ult} (1 + \varepsilon_{ult}) \tag{4}$$

where S_{ult} = Engineering Stress = $\frac{P_R}{A_o}$ (lbs/in^2)

$$\varepsilon_{ult} = \frac{\Delta l_{ult}}{l_o} \text{ (in/in)}$$

d. True Strain at Ultimate Load (ϕ_{ult})

$$\phi_{ult} = \ln (1 + \varepsilon_{ult}) \tag{5}$$

In practice $\varepsilon_{.002}$ is very small (less than .005 in/in for EC aluminum) and therefore $\phi_{.002} \approx \varepsilon_{.002}$ and $\sigma_{.002} \approx S_{.002}$.

Extended true stress-true strain curves were plotted in the manner described by Wistreich[13], as followed by Avitzur[11]. In this treatment the tensile test data obtained from specimens at all reductions by a given process are plotted on a single stress-strain diagram. The origin of an individual true stress-true strain curve is offset on the abscissa (true strain) by an amount corresponding to the true strain obtained by prior deformation. The envelope of these individual curves becomes the extended true stress-true strain curve. Redundant and frictional deformation are ignored in this treatment, but could be incorporated in a more exact analysis.

2. Density Measurements

The densities of the annealed, undeformed aluminum and the as extruded and as drawn specimens were measured using a differential weighing technique similar to those described by Bell[14] and Rogers

and Coffin[15]. The differential weighing technique consisted of weighing the specimen in air, weighing it suspended in liquid on a suitable holder, and weighing the holder alone, suspended in the liquid. The weighings were performed on a single pan microgram balance. The liquid used in this study was diethylene glycol monoethyl ether, chosen because of its high density, low surface tension, low vapor pressure, and its successful use in other studies[16]. The density of the liquid was measured as a function of temperature using the piknometer technique, with distilled water as the known liquid. The results are shown in Figure 2 and Table 5.

The specimen holder consisted of a .045 inch diameter aluminum frame suspended from the hook of the balance by a .003 inch diameter teflon coated wire, arranged so that only the .003 inch diameter wire was present at the air-liquid interface. Each time a weighing was made in liquid the depth of the specimen was adjusted so that the air-liquid interface intercepted the .003 inch diameter wire at the same point on the wire.

A series of weighings consisted of weighing a set of specimens (extruded or drawn) in air at least two times each specimen, and then weighing the set in liquid, again at least two times per specimen. In the latter case the empty holder was weighed suspended in the liquid (to the same depth) at frequent intervals. A total of 24 series of weighings were performed.

A series of weighings was usually completed in approximately

two hours and the density of the air was considered constant for a given series. In some cases the series of weighings was performed in the reverse order. Air temperature, humidity, and barometric pressure were recorded prior to and after each series of weighings in order to establish the density of the air. Liquid temperature was monitored continuously during the liquid weighings, and each specimen was allowed to stablize thermally in the liquid before a reading was taken. Specimens were stored in the same liquid in a container adjacent to the weighing container throughout the liquid weighing portion of a series.

The density of a specimen (D) was calculated at the temperature at which it was weighed using the following relationship:

$$D = \frac{W_a\, d_l - W_l\, d_a}{W_a - W_l} \qquad (6)$$

where, W_a = weight of specimen in air

W_l = weight of specimen in liquid

d_l = density of liquid

d_a = density of air

All densities were then corrected to 22°C for comparison purposes. Tables 6, 7 and 8 show the compilation of this data.

3. Metallography

Specimens of drawn and extruded wire were prepared for optical microscopy by mounting longitudinal sections in a room temperature cured epoxy. Rough grinding was then done with 320 through 600

grit wet paper and rough polishing accomplished using nine, three and one micron diamond paste. The specimens were then electro-polished using a solution of 78 ml perchloric acid, 120 ml distilled water, 700 ml ethanol and 100 ml ethylene glycol monobutyl ether. Polishing time was three seconds for all specimens with a polishing voltage of 12 volts for the .020 inch diameter ($\phi \approx 5.9$) specimens and 20 volts for the .045 inch diameter ($\phi \approx 4.1$) specimens. The specimens were then anodized using a solution of fluoroboric acid. Anodizing was performed at 30 volts for all specimens and the time consisted of eight to ten cycles, ten seconds on and ten seconds off, to prevent overheating of the specimen. Photomicrographs were taken on the Leitz MM5 metallograph using polarized light and a gypsum filter.

III. RESULTS AND DISCUSSION

An analysis and interpretation of the results emanating from this study will be presented in this section. Included will be discussions of the mechanical properties of the drawn and hydrostatically extruded products, extrusion pressure and die angle, density measurements, photomicrographs, and the temperature rise encountered in hydrostatic extrusion, in that order.

A. Mechanical Properties

The extended true stress - true strain curves for the drawn and hydrostatically extruded products are shown in Figures 3 through 6. In all cases the points shown are the averages of the individual tests shown in Tables 1 through 4, grouped by true strain. Figures 3 and 4 show the 0.2 percent offset true yield stress as a function of true strain, with Figure 4 being on logrithmic coordinates. The 0.2 percent offset true yield stress of both the drawn and extruded material is seen to increase in a regular manner with true strain, up to a true strain of approximately 2.3. Since both the drawn and the extruded curves appear approximately linear on the logrithmic coordinates up to a true strain of 2.3, they may be represented by an equation of the form $\sigma_{.002} = K \phi^{n}$ up to this point. The yield strength of the extruded product is never less than that of the drawn, up to a true strain of approximately 2.3, as has been observed by other investigators[5]. This may be due to the suppression of crack and void formation during hydrostatic extrusion. (See Section III C). The curve of the drawn material exhibits an

apparent discontinuity between true strains of approximately 2.3 and 3.5. The reason for this phenomenon is not clear, however, it cannot be ignored. At true strains greater than 3.5, the material continues to strain harden at a rate greater than that observed between true strains of 1.0 and 2.3. It has been suggested[16,17] that the yield strength of fcc materials saturates when cold worked to large true strains. This is not evident from this study, in fact, examination of the data shown in Tables 1 through 4 reveals that in all tensile tests the following conditions exist:

1. Elongation at ultimate load is always greater than that at 0.2 percent offset.
2. True stress at ultimate load is always greater than that at 0.2 percent offset.

Because of these conditions, and the fact that examination of the load-displacement diagrams shows that the load increaes monotonically with displacement, up to ultimate load, it is obvious that this material strain hardens when cold worked to true strains greater than 5.8.

The 0.2 percent offset true yield stress of the extruded material shows a pronounced decrease at true strains greater than 2.5. The major cause for this decrease in as extruded yield strength is due to recovery and recrystallization of the material as a result of the heat generated by the high reductions and final

velocities encountered. (See Sections III D and III E).

Figures 5 and 6 show the true stress at ultimate load as a function of true strain, with Figure 6 being on logrithmic coordinates. These curves are of essentially the same form as Figures 3 and 4, with the exception that the logrithmic plot of the drawn material property does not exhibit as noticeable a discontinuity as did its yield strength, and can probably be characterized by an equation of the form $\sigma_{ult} = K \phi^{n}$ over its entire length. It should also be noted that the true stress at ultimate load of the extruded material at a true strain of 5.87 is less than that of the annealed material.

Percent elongation at ultimate load as a function of true strain is shown in Figure 7 for both extruded and drawn wires. The gage length for all specimens was ten inches and in most cases the elongation of the drawn product is higher than the extruded. The elongation of the extruded specimens does not increase at large reductions as would be expected based on their decrease in tensile strengths. This would indicate that recovery and the initial stages of recrystallization are not significant in restoring ductility to this material and that there is, in fact, a lag in time between the inception of the loss of tensile strengths and the inception of the increase in ductility, at least for the combination of time and temperature encountered here. Even at a true strain of 5.87, where the true stress at ultimate load is less than that of the annealed material,

the elongation has not responded. Percent elongation at fracture as a function of true strain is shown for both processes in Figure 8. Here, the general trend is similar to percent elongation at ultimate load. In both cases the discontinuity observed in tensile properties of the drawn specimen is reflected in elongation.

B. Extrusion Pressure and Die Angle

The relationship between average extrusion runout pressure and true strain is shown in Figure 9. This curve generally reflects the prediction of equation 11.1 of Avitzur[11] as shown in his Figure 11.12. It should be noted, however, that at true strains near zero the experimental curve behaves somewhat differently. This discrepancy is caused by the fact that equation 11.1 uses the assumption of constant shear factor, m, and is not valid at true strains near zero because the critical angle for dead zone formation approaches zero in this area. Since the actual angle is then greater than the critical, a dead zone is predicted, and equation (11.6) governs and predicts higher pressures than realized experimentally. Equation (11.3), which considers hydrodynamic lubrication, should be used for comparison with the experimental data (See Section III E). Adequate data was not obtained to establish the optimum cone angle at any reduction. When hydrodynamic lubrication prevails, the optimum cone angle is affected not only by the reduction taken, but by the final velocity of the extrusion and the viscosity of the liquid. The viscosity is a function of temperature and pressure which are, in turn, affected by the final velocity. Cartwright[18] has shown that increasing the final

velocity, all other conditions being equal, results in an increase in extrusion pressure and a decrease in as extruded tensile strengths. This may be a result of strain rate effects on the flow stress of the material, the velocity increase itself, changes in the viscosity of the liquid, or, most probably, a combination of all three factors. Thermal softening of the material caused by the higher final velocity and temperature does not result in lower extrusion pressure as might be expected.

Figure 10 shows the effect of cone angle on the surface of the extruded wire. These extrusions were made at nearly the same final velocity, however, the smaller cone angles have provided better lubrication resulting in a corrugated finish on the wire. Larger cone angles, at this final velocity, have limited the amount of liquid flowing through the die, resulting in a shinier, burnished product and, therefore, shorter die life. If a higher final velocity was used with the larger cone angles, a corrugated surface could probably be obtained there as well. There was no noticeable change in mechanical properties as a result of this surface difference. In general, cone angles for hydrostatic extrusion are low, however, factors such as final velocity, liquid viscosity, density and heat capacity, metal heat capacity and flow stress and how these factors are affected by temperature, pressure and strain rate must be considered in order to predict the optimum cone angle and extrusion pressure required.

C. Density

The relationship between average relative density and true strain is shown in Figure 11 for both drawing and hydrostatic extrusion. The points shown here are relative to the measured density of the annealed material. The measured densities relative to the theoretical density of the material could not be obtained, since midway through the measurements it became apparent that the density of the liquid in which the specimens were weighed was itself changing with time due to some variable other than temperature. The cause of this change was never established, and therefore an absolute density of the aluminum could not be determined, but only relative density over a short period of time, i.e., one series of weighings. For this reason the density of each specimen in a series of weighings was made relative to the annealed specimen in that series and these relative densities were averaged over all series. Figure 11 shows a regular trend in relative density for both the drawn and extruded material. It appears that the higher hydrostatic stress state encountered in extrusion does, in fact, suppress the formation and even close up cracks and voids during deformation. The effect is slight, however, it does exist and is distinguishable from the drawn material, which is essentially unchanged. The increase in density of the extruded material may help explain the reason that the tensile strengths of the extruded material are never less than the drawn at true strains less than 2.3. Since the density of the extruded specimens increases beyond a true strain of 2.3, the

decrease in tensile strengths in this range does not appear to be caused by voids and microcracks.

D. Photomicrographs

Figure 12 shows 500X photomicrographs of the drawn and extruded material at true strains of approximately 4.0 and 5.8. It is evident from Figure 12, D that recrystallization of the highly elongated grains deformed by hydrostatic extrusion has begun. This is the primary reason for the decrease in tensile properties of the highly strained material. The path that the flow stress of the material follows as it travels through the die toward a true strain of 5.87 is not completely clear. It is postulated that the material work hardens rapidly through the die and only after emerging from the die has enough time elapsed for recovery and recrystallization to be effective. This is based on the observation that the highly elongated grains are still evident in the recrystallized structure. The average extrusion runout pressure (Figure 9) shows no effect of a lower flow stress during extrusion. Apparently the decrease in flow stress caused by the increase in temperature during extrusion is offset by the increase in flow stress caused by strain rate and by the size effect of the smaller final diameters.

The photomicrographs of the drawn material and the material extruded to a true strain of 4.1 show no signs of recrystallization. This would indicate that the reason for the decrease in tensile strengths of the material extruded to a true strain of 4.1 is due to the recovery mechanism.

E. Theoretical Consideration of Temperature Rise

In conventional extrusion Johnson and Kudo[19] state that heat conduction may be negligible when extrusion speeds exceed about 1.0 inch/second. In hydrostatic extrusion there may be even less opportunity for heat conduction away from the deformation zone of the billet since, ideally, the only point of possible contact between the billet and the tooling is at the die and here a layer of fluid separates the two. Since no dead zone appears to exist in this study, see Figure 10, there is no static metal buildup behind the die to permit heat transfer at this point. For these reasons we will consider hydrostatic extrusion at high velocity to be an adiabatic process, and the aluminum and the fluid to be two separate adiabatic systems, at least while in the deformation zone of the die. The analysis of Avitzur, originally presented in Reference 20 will be utilized. When hydrodynamic lubrication prevails, the thickness of the lubricant layer (ϵ) at the die land (L), see Figure 13, is given by Avitzur's[11] equation (n) and (8.41) page 187 as:

$$\frac{\epsilon}{R_f} = \sqrt{\frac{v_f \ \eta_f}{R_f \ \sigma_{of}} \ \frac{1}{f(\alpha)} \left\{ \frac{\cot \alpha \cos^2 \alpha}{3} \left[1 - \left(\frac{R_f}{R_o} \right)^3 \right] + \frac{L}{R_f} \right\}} \qquad (7)$$

where, R_f = final radius of die

R_o = initial radius of billet = .1826 inch

v_f = final velocity of extrusion

η_f = viscosity of fluid at R_f

σ_{of} = flow stress of material at R_f

α = die semi-cone angle

L = die land = 0.010 inch

$$f(\alpha) = \frac{1}{\sin^2\alpha}\left[1 - (\cos\alpha)\sqrt{1 - \frac{11}{12}\sin^2\alpha} + \frac{1}{\sqrt{11\cdot 12}}\cdot\ln\frac{1+\sqrt{\frac{11}{12}}}{\sqrt{\frac{11}{12}}\cos\alpha + \sqrt{1 - \frac{11}{12}\sin^2\alpha}}\right] \quad (8)$$

The dimensionless ratio $\frac{\epsilon}{R_f}$ is calculated by successive approximations for each combination of R_f, v_f, α and L desired.

In this study the flow stress of the aluminum at R_f is estimated by:

$$\sigma_{of} = 15{,}500\ (.0015 + \phi)^{.225}\ \text{lbs/in}^2$$
$$= 15{,}500\left(.0015 + 2\ln\frac{R_o}{R_f - \epsilon}\right)^{.225}\ \text{lbs/in}^2 \quad (9)$$

which is an approximation of the data obtained by cold drawing. Flow stress σ_{of} is dependent on ϵ, since the final radius of the product is $R_f - \epsilon$, not R_f, although ϵ may be disregarded here since it is small.

The viscosity of the fluid at R_f is approximated by:

$$\eta_f = (8.47 - .021\ TF_f) \times 10^{-5}\ \frac{\text{lb-sec}}{\text{in}^2} \quad (10)$$

where TF_f is the final temperature of the fluid. This expression was estimated from data provided by Cartwright[18], in conjunction with that shown by Streeter[21]. The temperature rise in the fluid must be determined in order to establish η_f. Equations (i) and (j)

page 186 of reference 11 are utilized. Equation (i) gives the upper bound of power required to shear the fluid across the conical die surface, Γ_3, as:

$$\dot{W}_{s3} = \frac{2}{3} \pi v_f^2 R_f^2 \cot\alpha (\cos^2\alpha) \frac{\eta}{\epsilon}\left[1 - \left(\frac{R_f}{R_o}\right)^3\right] \quad (11)$$

where, η = average viscosity of fluid

$$\dot{V} = \pi v_f R_f^2$$

$$\dot{W}_{s3} = \frac{2}{3} \dot{V} v_f \cot\alpha (\cos^2\alpha) \frac{\eta}{\epsilon}\left[1 - \left(\frac{R_f}{R_o}\right)^3\right] \quad (12)$$

The work required is:

$$W_{s3} = \int_t \dot{W}_{s3}\, dt$$

$$W_{s3} = \frac{2}{3} V v_f \cot\alpha (\cos^2\alpha) \frac{\eta}{\epsilon}\left[1 - \left(\frac{R_f}{R_o}\right)^3\right] \quad (13)$$

This is then converted to heat and the temperature rise calculated as follows:

$$Q_{s3} = \frac{W_{s3}}{12J}$$

$$\Delta T_{s3} = \frac{Q_{s3}}{C_p \rho V}$$

$$\Delta T_{s3} = \frac{\frac{2}{3} v_f \cot\alpha (\cos^2\alpha) \frac{\eta}{\epsilon}\left[1 - \left(\frac{R_f}{R_o}\right)^3\right]}{12 J C_p \rho} \quad (14)$$

where, J = mechanical equivalent of heat

$$= 778 \frac{\text{ft-lb}}{\text{BTU}}$$

C_p = heat capacity of fluid[22]

$= 0.5 \frac{BTU}{lb°F}$

ρ = density of fluid[22] = $.032 \frac{lb}{in^3}$

so that,

$$\Delta T_{s3} = \frac{v_f \cot\alpha \ (\cos^2\alpha) \frac{\eta}{\epsilon}\left[1 - \left(\frac{R_f}{R_o}\right)^3\right]}{224.1} \qquad (15)$$

Since the actual radius of the extrusion is $R_f - \epsilon$, equation (15) becomes:

$$\Delta T_{s3} = \frac{v_f \cot\alpha \ (\cos^2\alpha) \frac{\eta}{\epsilon}\left[1 - \left(\frac{R_f - \epsilon}{R_o}\right)^3\right]}{224.1} \qquad (16)$$

Equation (j), page 186, reference 11 gives the power required to shear the fluid along the cylindrical surface of the die, Γ_4, as:

$$\dot{W}_{s4} = 2\pi v_f^2 R_f^2 \frac{L}{R_f} \frac{\eta}{\epsilon} \qquad (17)$$

When treated in a manner analagous to equation (11), this expression becomes:

$$\Delta T_{s4} = \frac{v_f \ L \ \eta}{74.7 \ (R_f - \epsilon)\epsilon} \qquad (18)$$

The final temperature of the fluid then becomes:

$$TF_f = T_o + \Delta T_{s3} + \Delta T_{s4} \qquad (19)$$

where, T_o = initial fluid temperature = 75°F.

Equations (7), (9), (10), (16), (18), and (19) are solved by successive approximations until compatible values of each

variable (ϵ, σ_{of}, η, η_f, and TF_f) are obtained for each combination of R_f, v_f, α and L desired.

An estimate of the temperature rise in the aluminum is obtained by using equations (8.11a) and (8.12), Reference 11. Equation (8.12) gives the upper bound on the power consumed along the two surfaces of velocity discontinuity Γ_1 and Γ_2. In the present analysis the power consumed along these surfaces is handled separately, with surface Γ_2 being treated first. Equation (8.12) becomes:

$$\dot{W}_{s2} = \frac{1}{\sqrt{3}} \sigma_o \pi v_f R_f^2 \left(\frac{\alpha}{\sin^2 \alpha} - \cot \alpha \right) \qquad (20)$$

where, $\sigma_o = 15{,}500 \ (.0015 + \phi)^{.225}$

$$\phi = 0.0$$

$$\dot{V} = \pi v_f R_f^2$$

$$\dot{W}_{s2} = \frac{3579}{\sqrt{3}} \dot{V} \left(\frac{\alpha}{\sin^2 \alpha} - \cot \alpha \right) \qquad (21)$$

The work required becomes:

$$W_{s2} = \int_t \dot{W}_{s2} \, dt$$

$$W_{s2} = \frac{3579}{\sqrt{3}} V \left(\frac{\alpha}{\sin^2 \alpha} - \cot \alpha \right) \qquad (22)$$

Converting this to heat, the temperature rise is calculated as follows:

$$Q_{s2} = \frac{W_{s2}}{12J}$$

$$\Delta T_{s2} = \frac{Q_{s2}}{C_p \rho V}$$

$$\Delta T_{s2} = \frac{3579\left(\frac{\alpha}{\sin^2\alpha} - \cot\alpha\right)}{\sqrt{3}\qquad 12J\ C_p\ \rho} \tag{23}$$

where, J = mechanical equivalent of heat

$$= 778\ \frac{\text{ft lb}}{\text{BTU}}$$

C_p = heat capacity of aluminum[23]

$$= .183 + .000011^{\circ}R\ \frac{\text{BTU}}{\text{lb}\ ^{\circ}R}$$

ρ = density of aluminum = $.097\ \frac{\text{lb}}{\text{in}^3}$

so that $$\Delta T_{s2} = \frac{3579\left(\frac{\alpha}{\sin^2\alpha} - \cot\alpha\right)}{905.6\quad C_p\quad \sqrt{3}} \tag{24}$$

This portion of the temperature rise is calculated by successive approximations with C_p being based on the average temperature.

Next, the temperature rise in the aluminum caused by the internal deformation is treated. Equation (8.11a) gives the power required as:

$$\dot{W}_i = 2\pi\sigma_o v_f R_f^2 f(\alpha) \ln\frac{R_o}{R_f} \tag{25}$$

By treating equation (25) in a manner analogous to that given equation (20), the temperature rise caused by internal deformation is:

$$\Delta T_i = \frac{2\sigma_o f(\alpha) \ln \frac{R_o}{R_f - \epsilon}}{C_p\ 905.6} \tag{26}$$

Since σ_o is a function of reduction, the temperature rise is calculated by breaking the conical portion of the material into segments so that

the increment in σ_o in any segment is less than some small number, say 1000 psi (see Figure 13.5). The average σ_o and the average C_p in any segment is then used to obtain the temperature rise in that segment. The average σ_o is taken to be the σ_o corresponding to the average true strain across the segment. The final σ_o in the last segment is σ_{of}, discussed earlier.

Finally, the temperature rise incurred at the second surface of velocity discontinuity, Γ_1, is obtained in a manner directly analogous to that at Γ_2. In this case σ_{of} is used as the flow stress of the aluminum. The final temperature of the aluminum then becomes:

$$TA_f = T_o + \Delta T_{s2} + \Delta T_i + \Delta T_{s1} \qquad (27)$$

The extrusion back pressure, P_b, was calculated simultaneously with the temperature rise using equation (11.3) of Reference 11, which reads:

$$\frac{P_b}{\sigma_o} = \frac{P_a}{\sigma_o} + 2\, f(\alpha) \ln\left(\frac{R_o}{R_f}\right) + \frac{2}{\sqrt{3}}\left(\frac{\alpha}{\sin^2\alpha} - \cot\alpha\right) + 2\,\frac{v_f \eta}{R_f \sigma_o}\left[\cot\alpha \cos^2\alpha \left(\frac{R_f}{R_o}\right)^3 + \frac{L}{R_f}\right] + 4\sqrt{\frac{v_f \eta}{R_f \sigma_o}\, f(\alpha)\left\{\frac{\cot\alpha \cos^2\alpha}{3}\left[1 - \left(\frac{R_f}{R_o}\right)^3\right] + \frac{L}{R_f}\right\}} \qquad (28)$$

where P_a = receiver pressure = 0

The results of the foregoing calculations are shown graphically in Figures 14 through 27 from which the following general observations may be made:

1. The calculated relationship (Equation (28)) between extrusion back pressure and true strain (Figures 14 and 15) generally predicts the results obtained experimentally (Figure 9), even at low values of true strain.
2. Optimum die angles are generally small, but increase with increasing final velocity. This is because the fluid gap ϵ becomes excessive with increasing velocity and small die angles, resulting in larger reductions and higher pressures. Increasing the die angle restricts the flow of fluid through the die because of the lower surface velocity of the extrusion along the conical portion of the die. This velocity is given as $v = v_f \, r_f^2 \, \frac{\cos \alpha}{r^2}$ which shows that as the die angle increases the surface velocity decreases and that the metal accelerates toward the exit of the die. At low final velocities (25 in/sec, Figure 19) the optimum angle appears to be less than 1°.
3. The aluminum final temperature and back pressure are affected only slightly by changes in cone angle and velocity.
4. Final velocity, cone angle and true strain all affect $\frac{\epsilon}{R_f}$ and the fluid final temperature, however, the temperature rise of the fluid is small. Both $\frac{\epsilon}{R_f}$ and TL_f increase sharply with decreasing cone angle as may

be expected, since the velocity across the cone increases with decreasing cone angle.

The theoretically calculated final temperature and back pressure corresponding to the experimental extrusion which showed signs of recrystallization are shown below:

	EXPERIMENT	THEORY
TA_f	-	555°F
P_b	144,000 lb/in^2	116,400 lb/in^2
v_f	500 in/sec	500 in/sec
Φ	5.87 in/in	5.87 in/in

The calculated values of back pressure and aluminum temperature may be somewhat low because the effect of strain rate on the flow stress of the aluminum was not considered.

IV. CONCLUSIONS AND RECOMMENDATIONS

Mechanical tests on as extruded E C aluminum show an initial increase in tensile strengths with increasing true strain, and then decreasing tensile strengths at true strains greater than 3.0 (See Figures 3 and 4 and Tables 1 and 4). This is a result of the higher temperatures encountered at higher true strains and final velocities (See Section III E). Theoretical analysis of the temperature rise encountered in hydrostatic extrusion reveals that the major influence on temperature is the amount of reduction taken, with final velocity and die cone angle having only slight effects (See Figures 16, 20 and 25). Velocity of extrusion would undoubtedly show a larger effect if the effect of strain rate on the flow stress of the material was considered in the analysis. The decrease in tensile strengths at high strain is attributed to recovery and recrystallization as revealed by metallographic examination (See Figure 12). The sharp decrease in tensile strengths at high strains is not accompanied by an increase in elongation, even when the true stress at ultimate load of the highly deformed material is approximately the same as that of the annealed material (See Figures 7 and 8). This indicates a time lag between the onset of the degradation of tensile strengths and the onset of the increase in elongation at the times and temperatures encountered in this process.

Mechanical tests on the specimens drawn at slow speeds show a continuous increase in tensile strengths for all true strains tested, except for an unexplained discontinuity at a true strain of approximately three (See Figures 3 and 4 and Tables 3 and 4).

Both the experimental and the theoretical work indicate that optimum die angles for hydrostatic extrusion are low, as a result of the low friction afforded by hydrodynamic lubrication (See Figures 9, 14, 15 and 19). The optimum die angle is affected by the reduction, final extrusion velocity, fluid viscosity and how it varies with temperature and pressure, and the material flow stress and how it varies with temperature, pressure and strain rate.

An analysis of the temperature rise in the fluid during extrusion shows it to be low. The temperature of the fluid increases with decreasing cone angle, increasing final velocity and increasing reduction (See Figures 17, 21 and 26).

Density measurements showed an increase in density of the hydrostatic extruded specimens for all true strains measured and essentially no change in density of the drawn specimens over the same range of true strains (See Figure 11 and Tables 6, 7 and 8).

A more sophisticated future study should consider in process material properties in a more complete manner. Specifically, consideration of the flow stress of the aluminum under varying conditions of hydrostatic stress, strain, strain rate and temperature would yield more precise temperature rise and extrusion pressure calculations. Similar treatment of the fluid viscosity under these varying conditions would be advantageous. Consideration might also be given to techniques for the improvement of elongation of the as extruded and as drawn material.

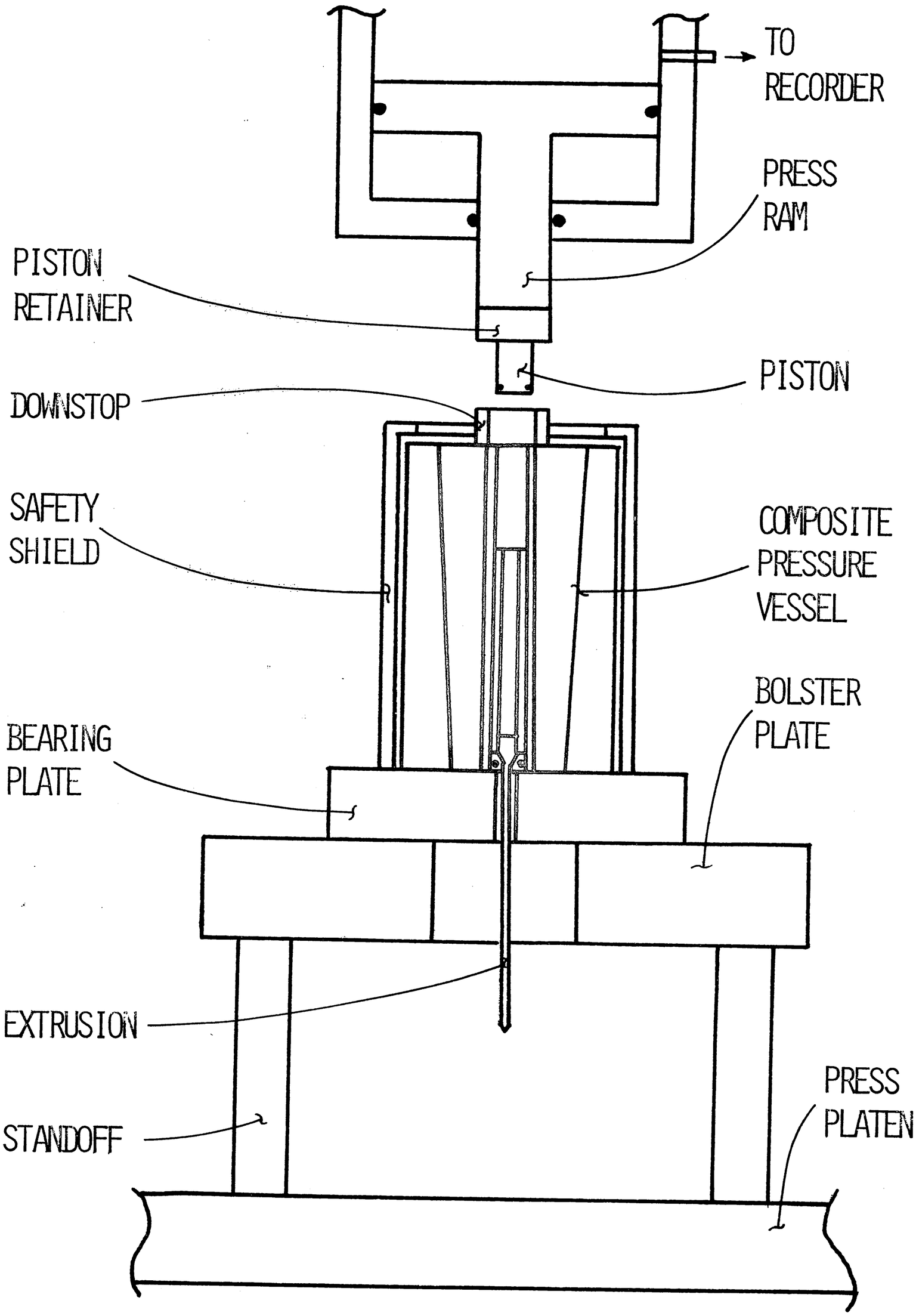

FIGURE 1

PRESSURE VESSEL AND PRESS

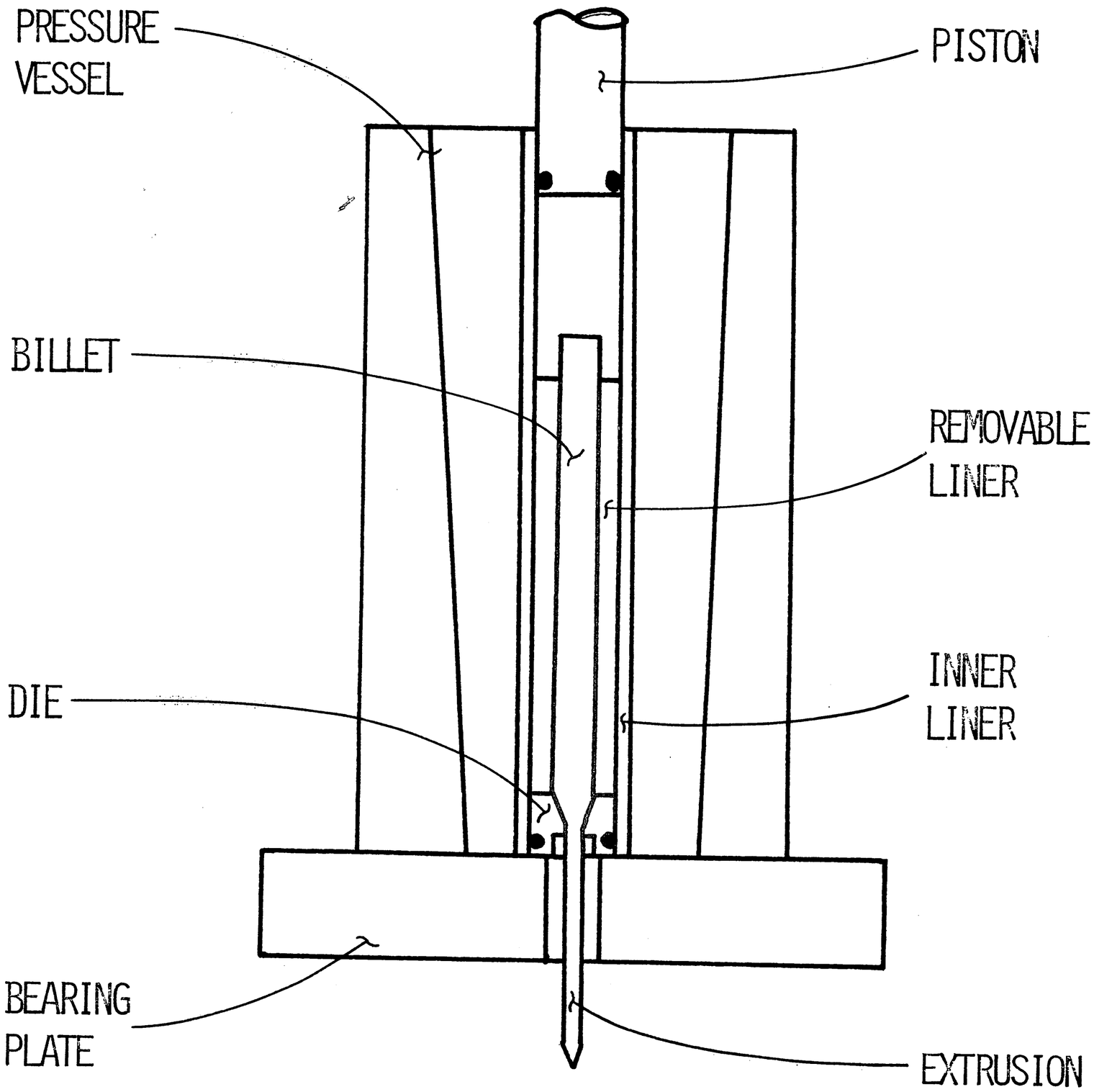

FIGURE 1 (CONT'D)

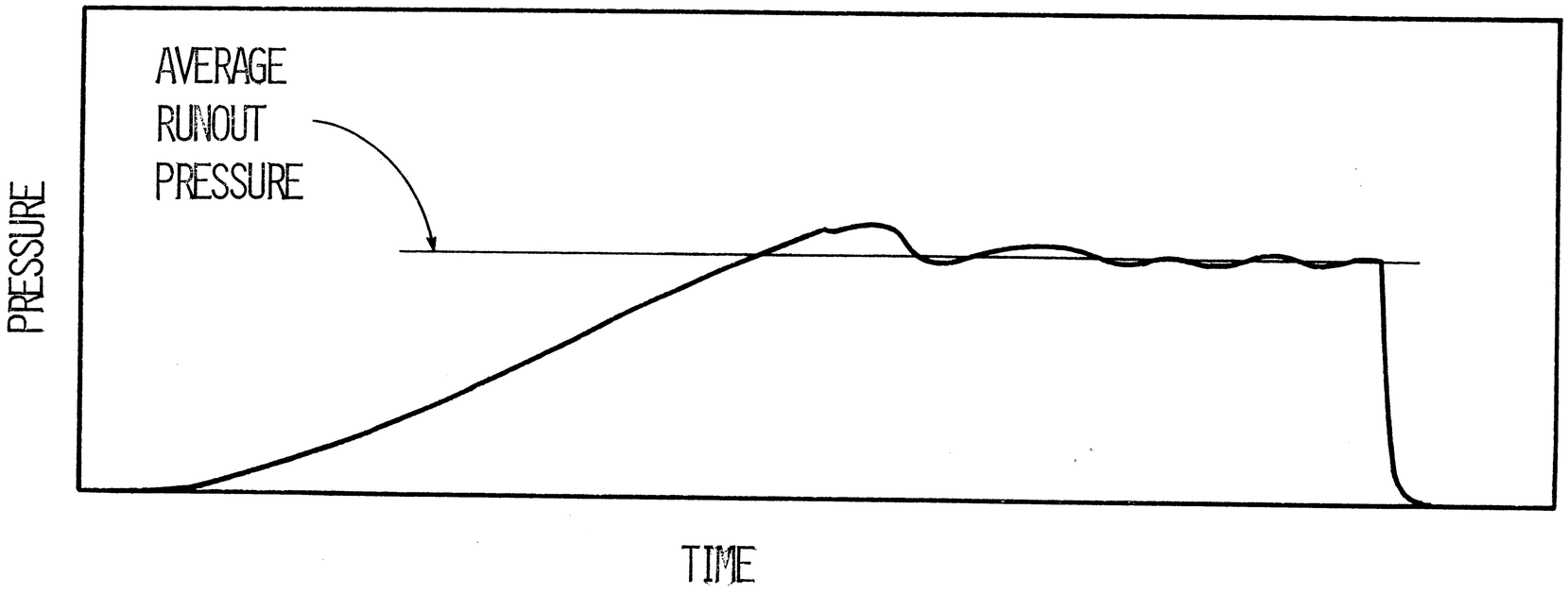

FIGURE 1.5 - TYPICAL PRESSURE VS TIME RECORDING

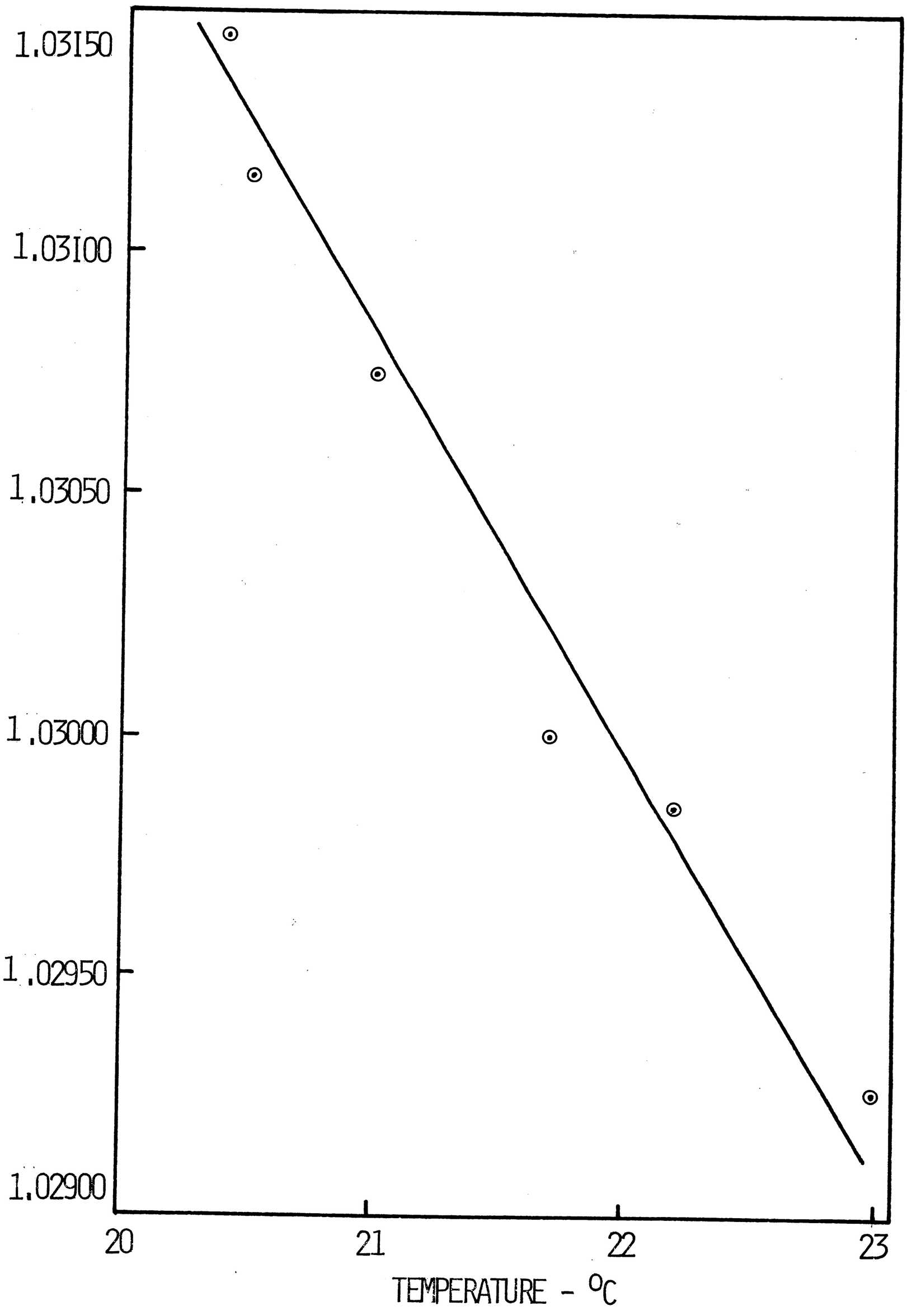

FIGURE 2 - DENSITY VS TEMPERATURE

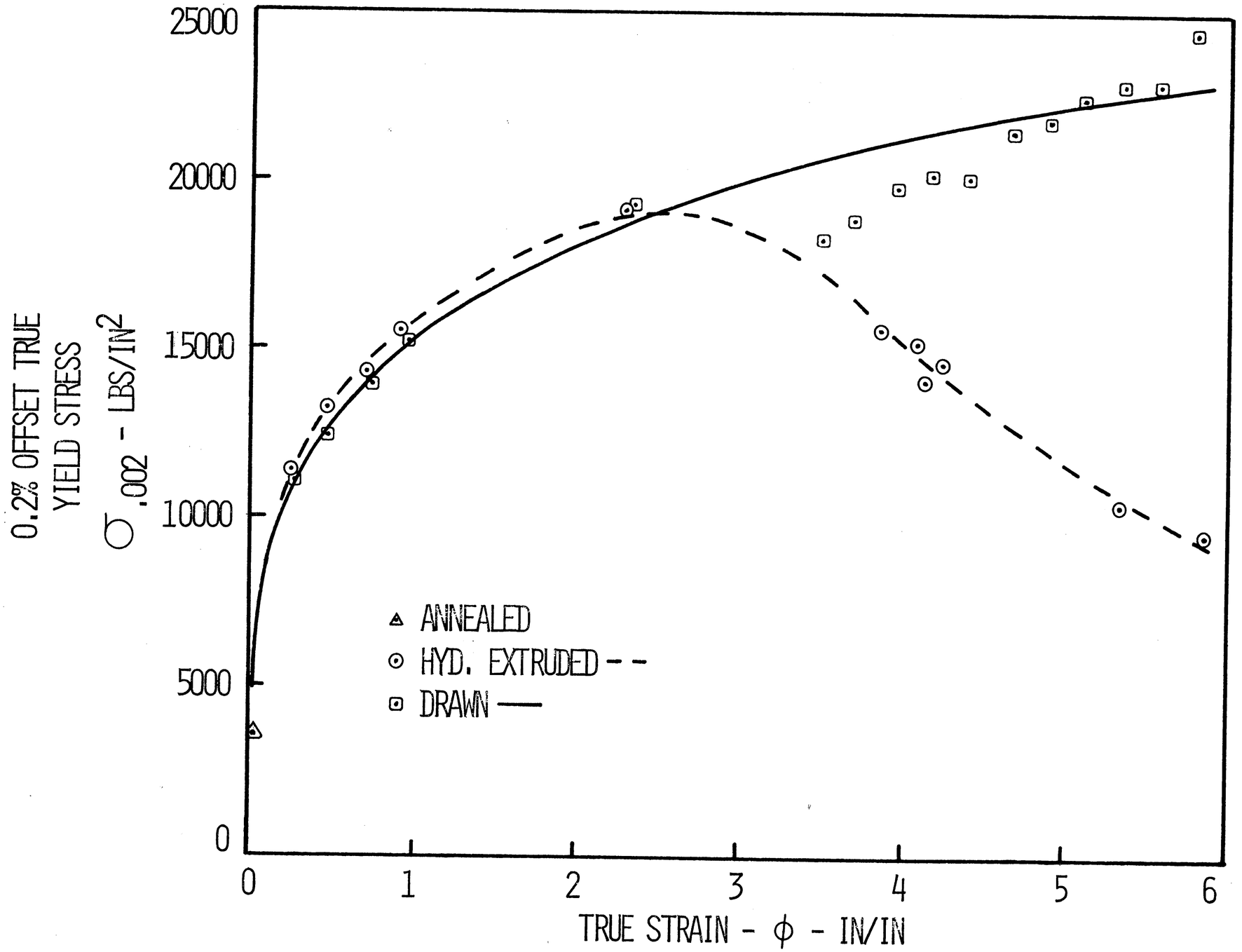

FIGURE 3 - EXTENDED TRUE STRESS VS TRUE STRAIN

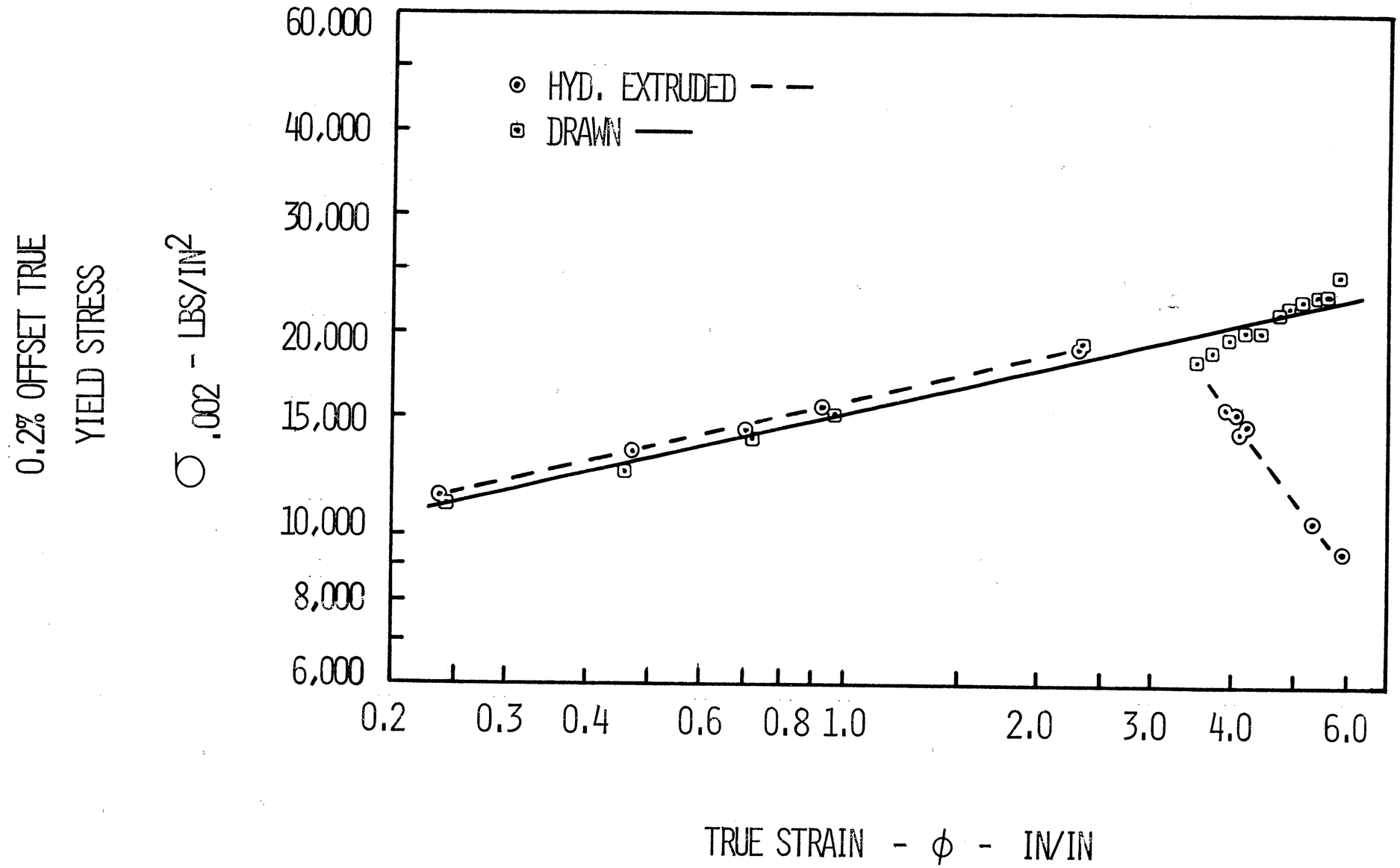

FIGURE 4 - EXTENDED TRUE STRESS VS TRUE STRAIN

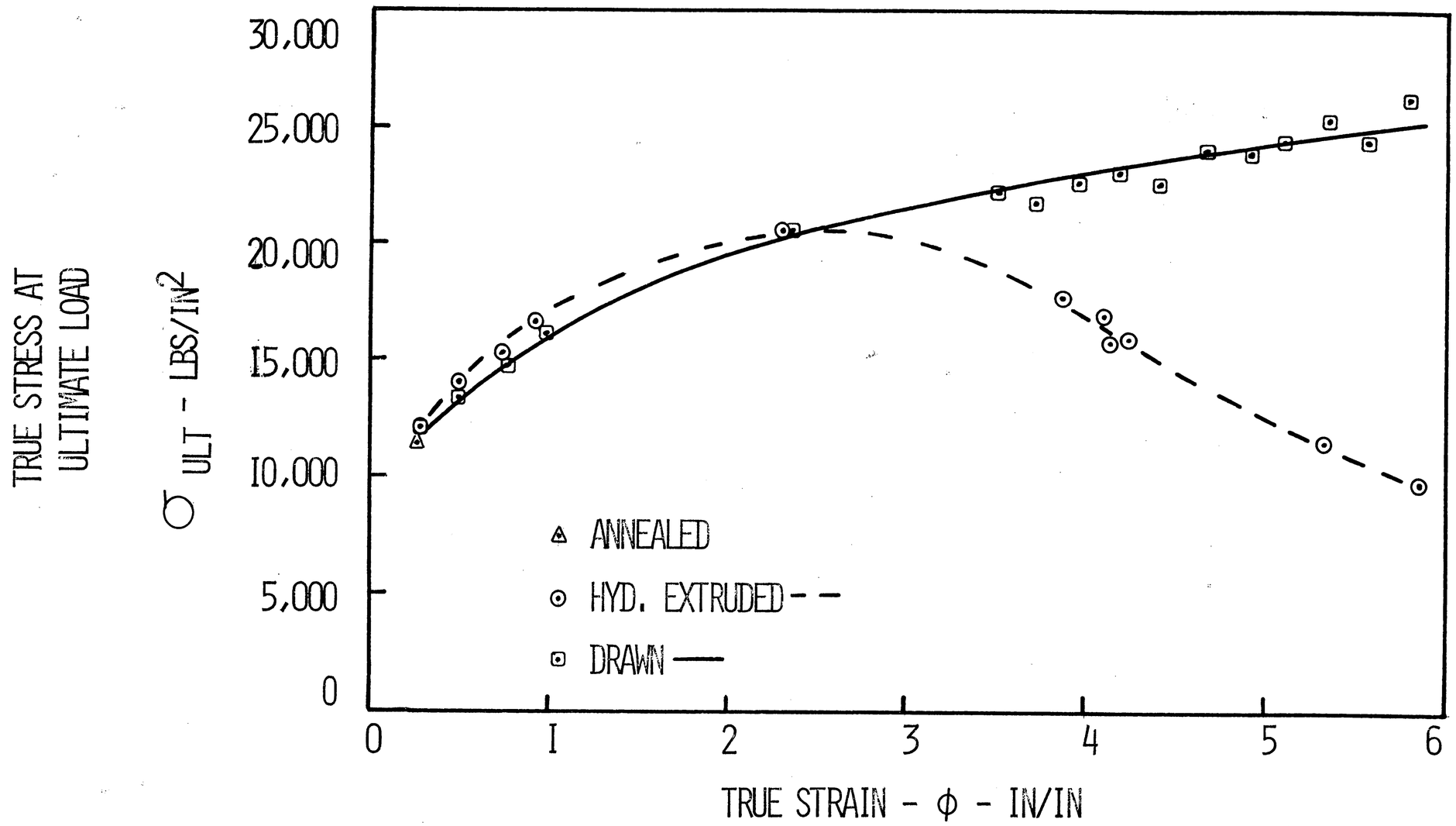

FIGURE 5 - EXTENDED TRUE STRESS VS TRUE STRAIN

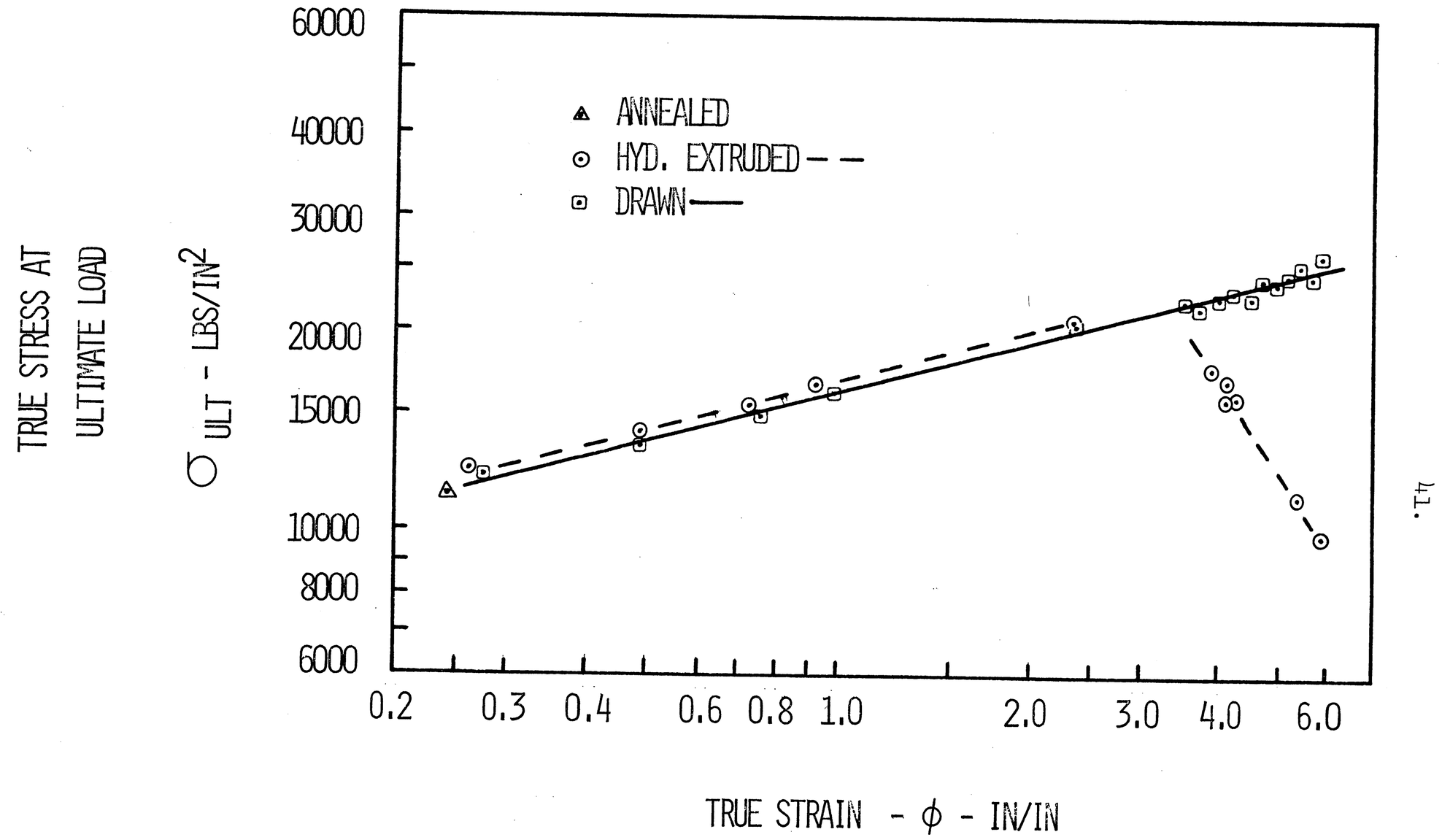

FIGURE 6 - EXTENDED TRUE STRESS VS TRUE STRAIN

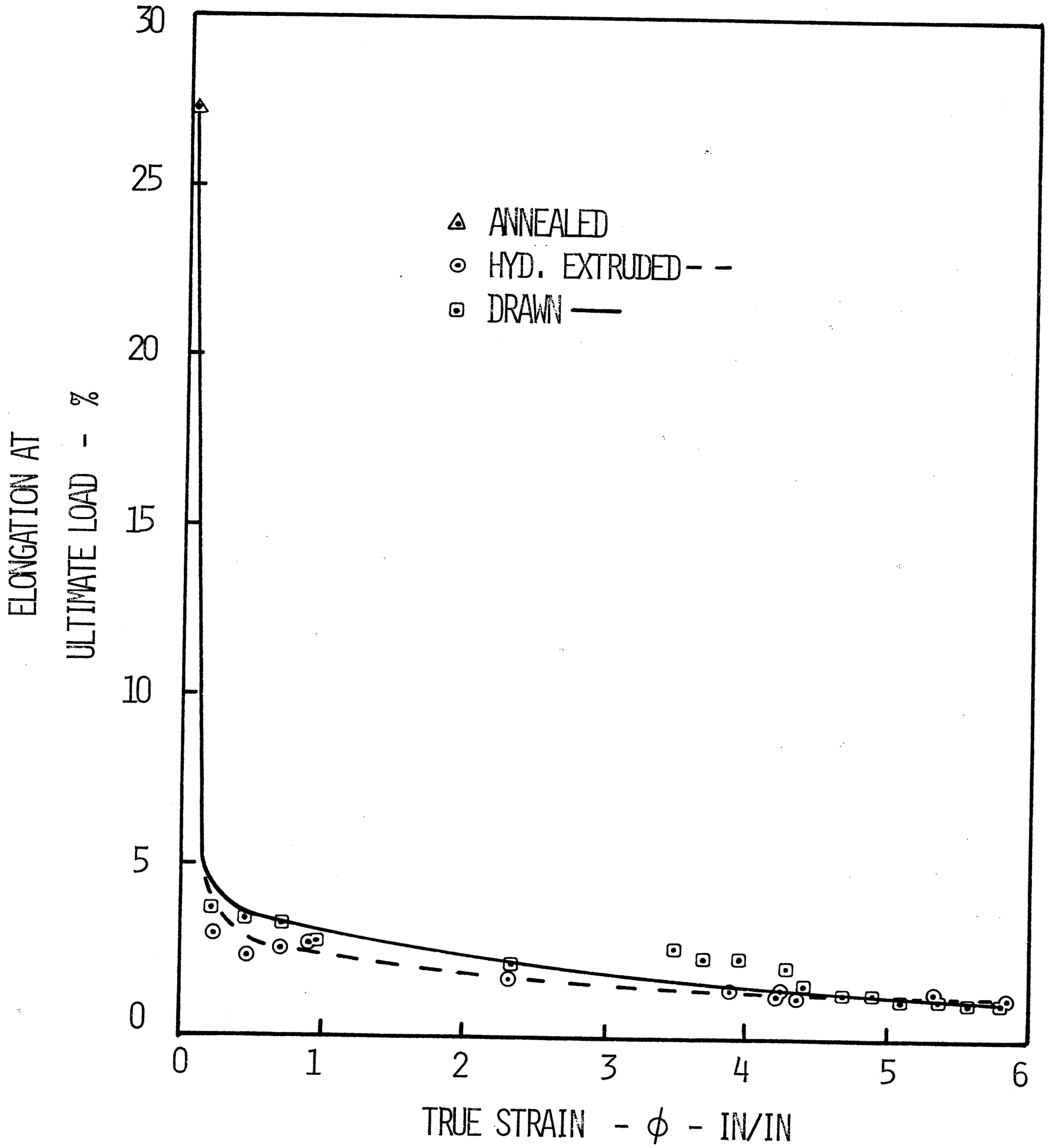

FIGURE 7 - ELONGATION VS TRUE STRAIN

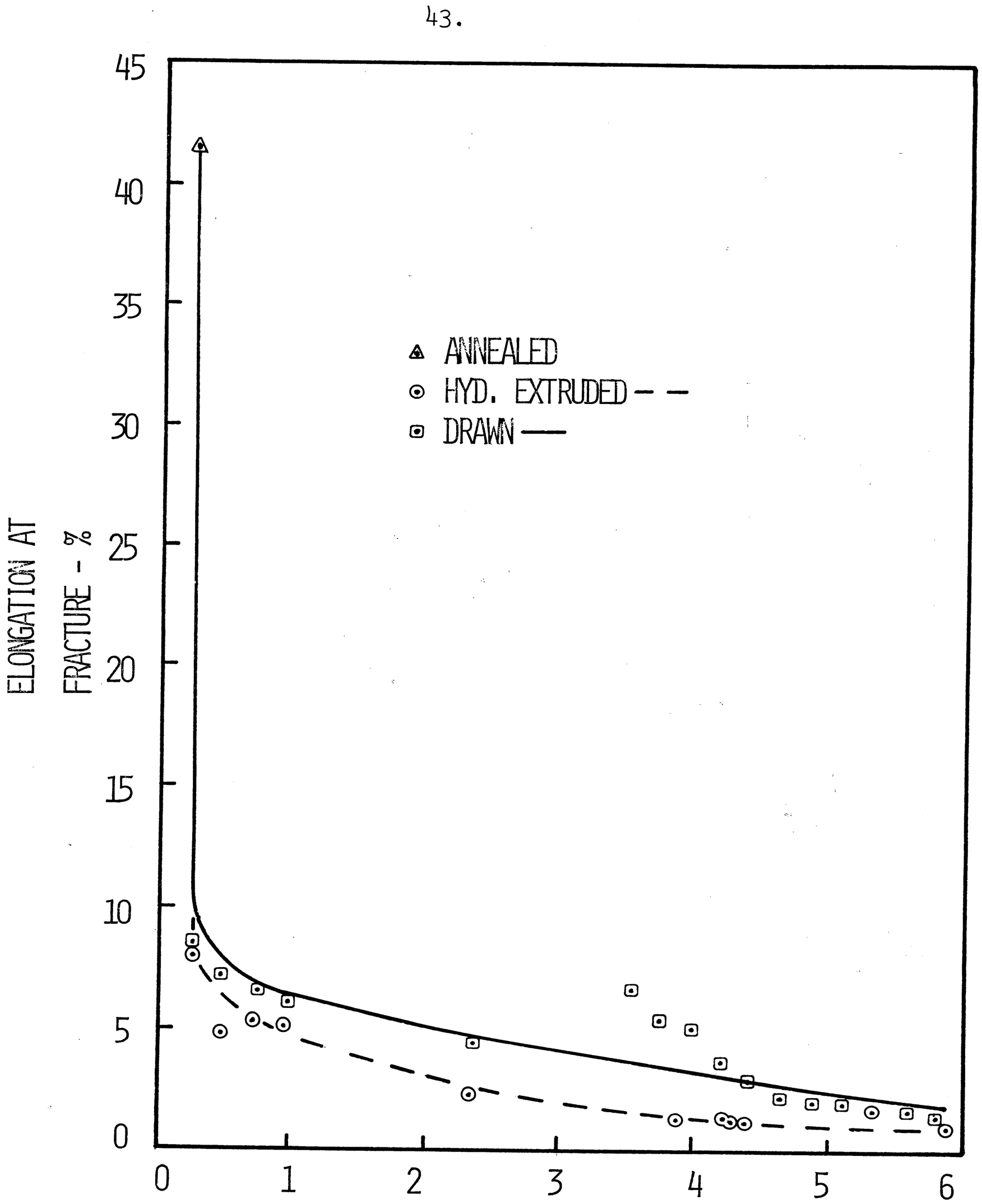

FIGURE 8 - ELONGATION VS TRUE STRAIN

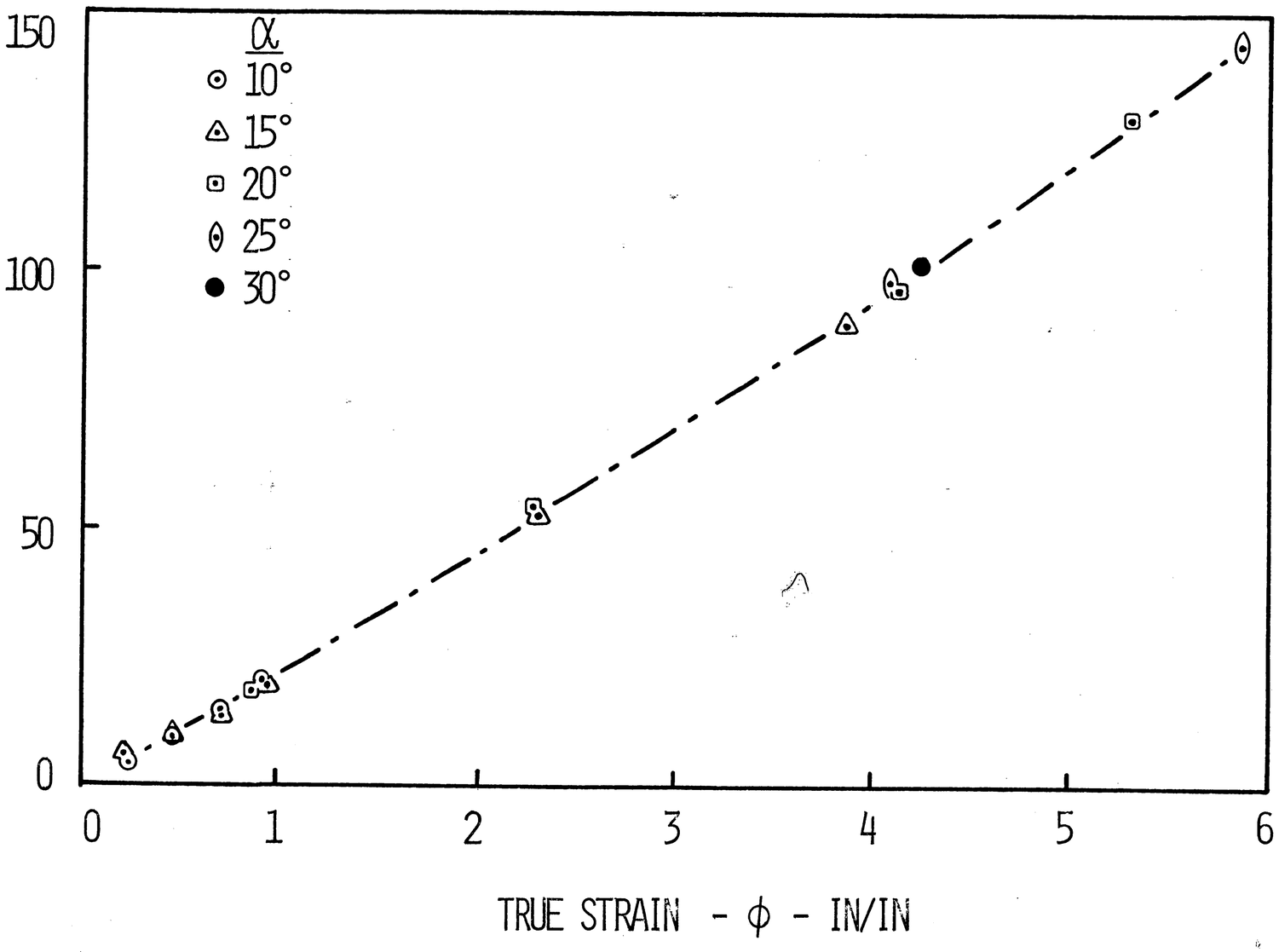

FIGURE 9 - TRUE STRAIN VS AVERAGE EXTRUSION RUNOUT PRESSURE

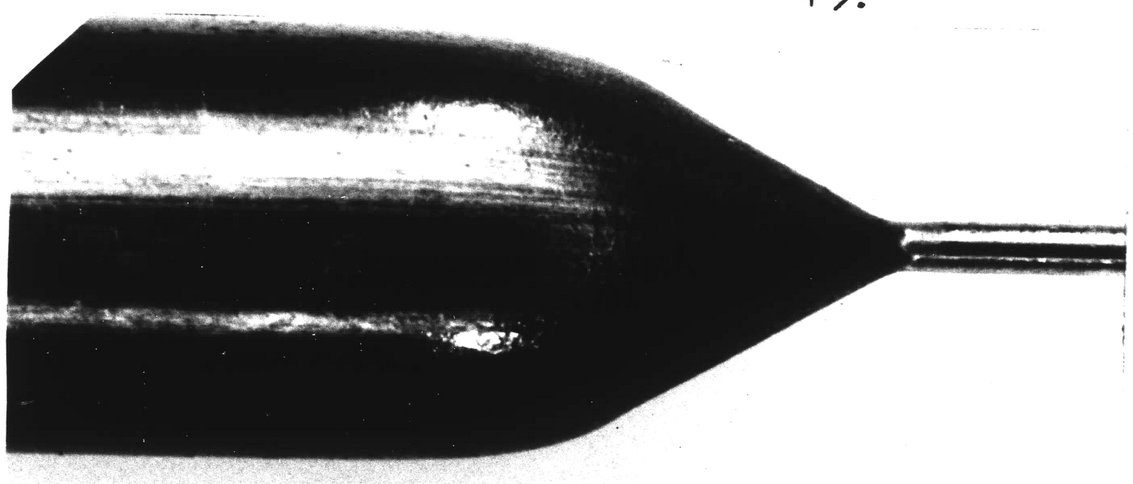

SEMICONE ANGLE
$\alpha = 30^{o}$
TRUE STRAIN
$\phi = 4.22$

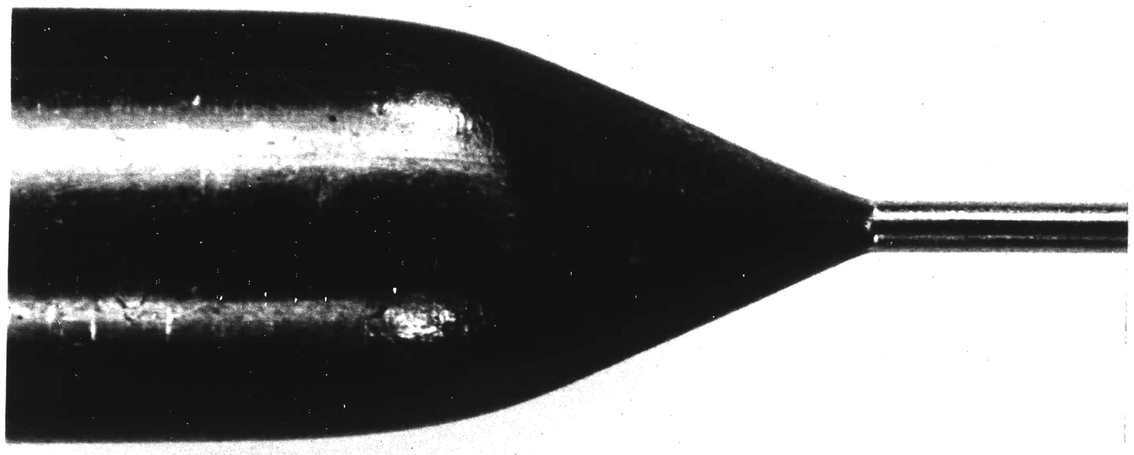

SEMICONE ANGLE
$\alpha = 25^{o}$
TRUE STRAIN
$\phi = 4.09$

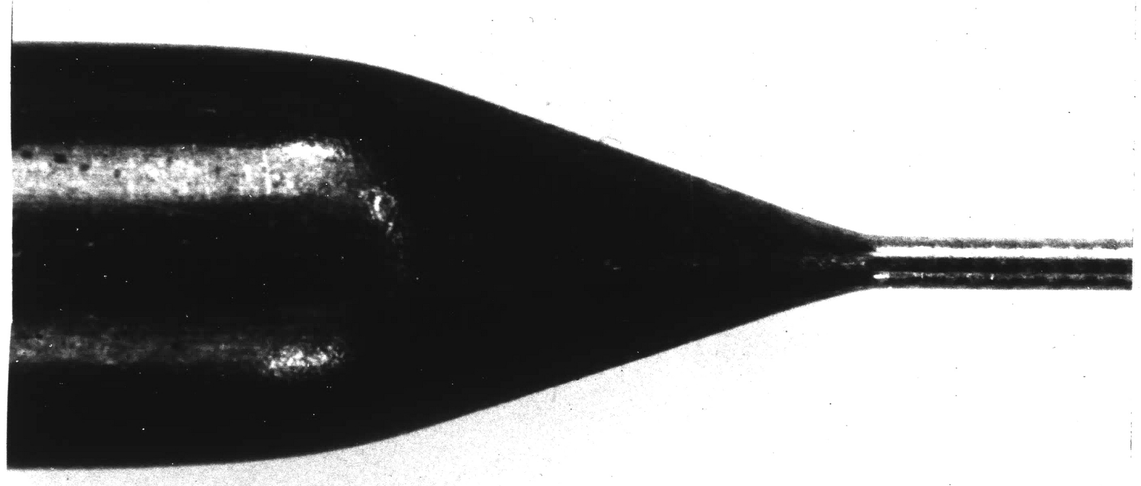

SEMICONE ANGLE
$\alpha = 20^{o}$
TRUE STRAIN
$\phi = 4.13$

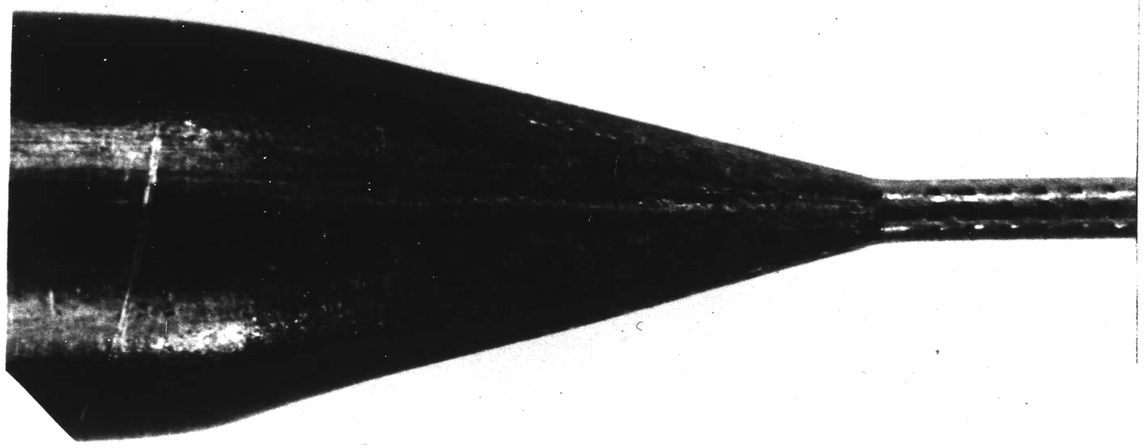

SEMICONE ANGLE
$\alpha = 15^{o}$
TRUE STRAIN
$\phi = 3.86$

FIGURE 10 - EFFECT OF CONE ANGLE ON WIRE SURFACE

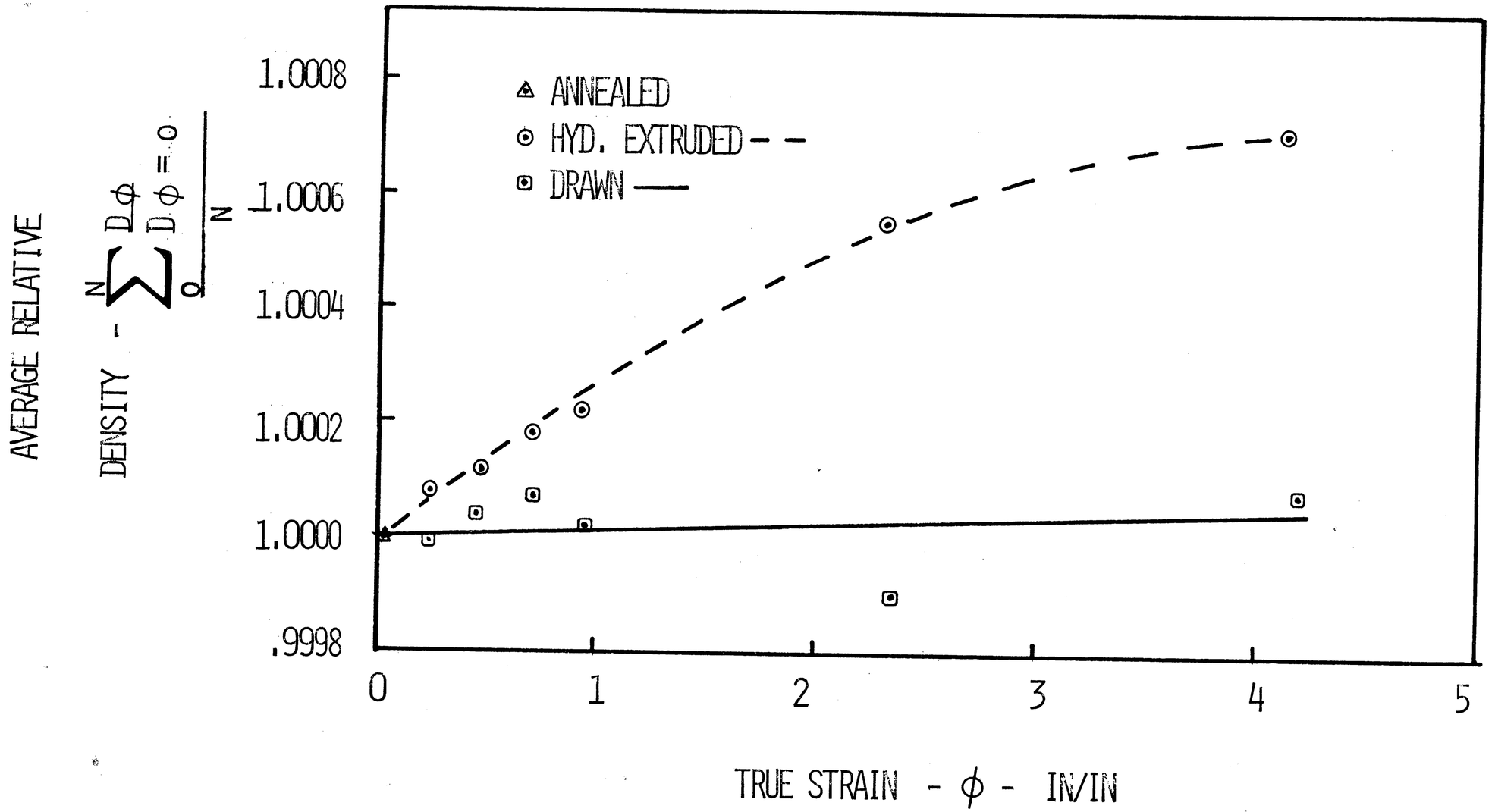

FIGURE 11 - TRUE STRAIN VS AVERAGE RELATIVE DENSITY

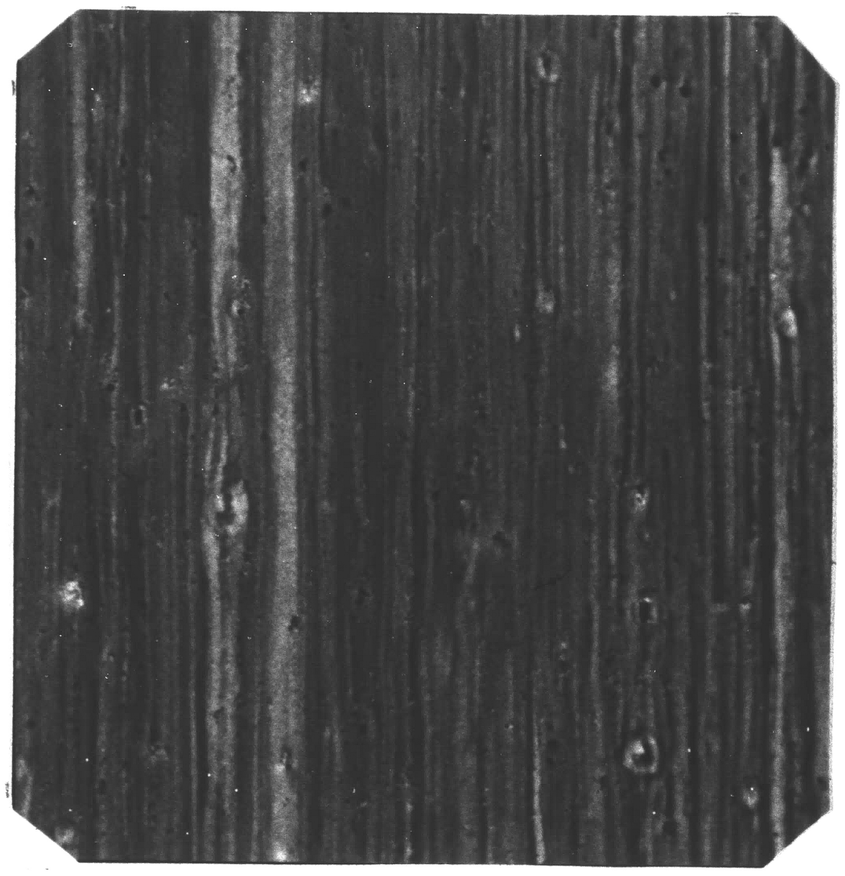

A. DRAWN

TRUE STRAIN - ϕ = 4.18 IN/IN

FINAL VELOCITY-V_f = 3.1 IN/SEC

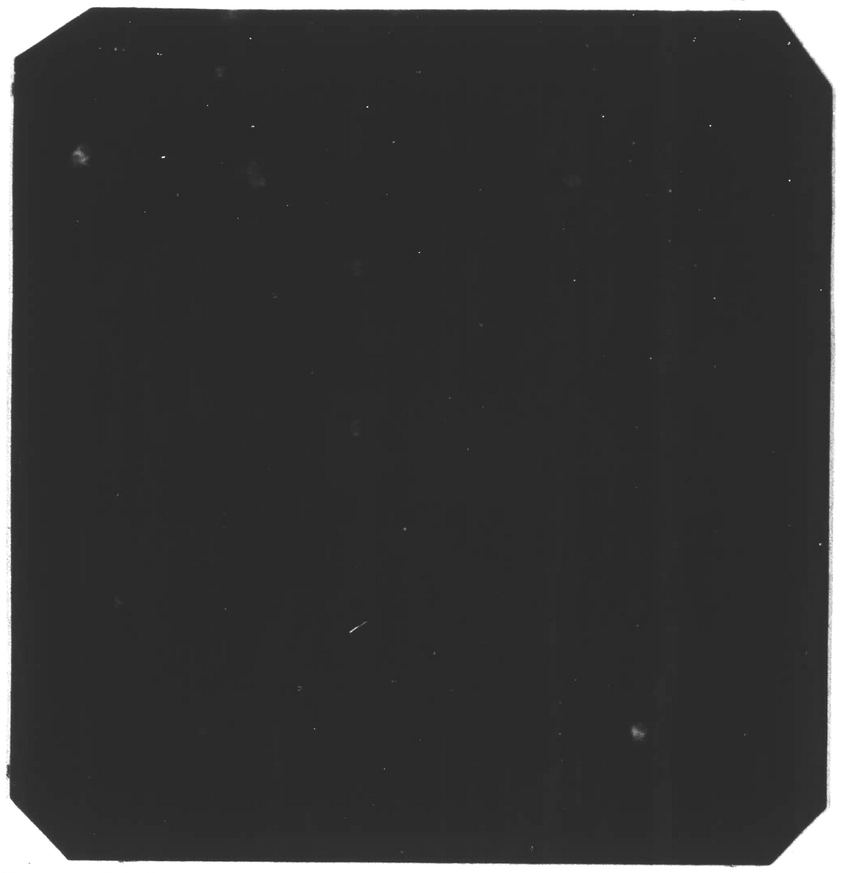

B. EXTRUDED

TRUE STRAIN -ϕ= 4.00 IN/IN

FINAL VELOCITY-V_f = 50 IN/SEC

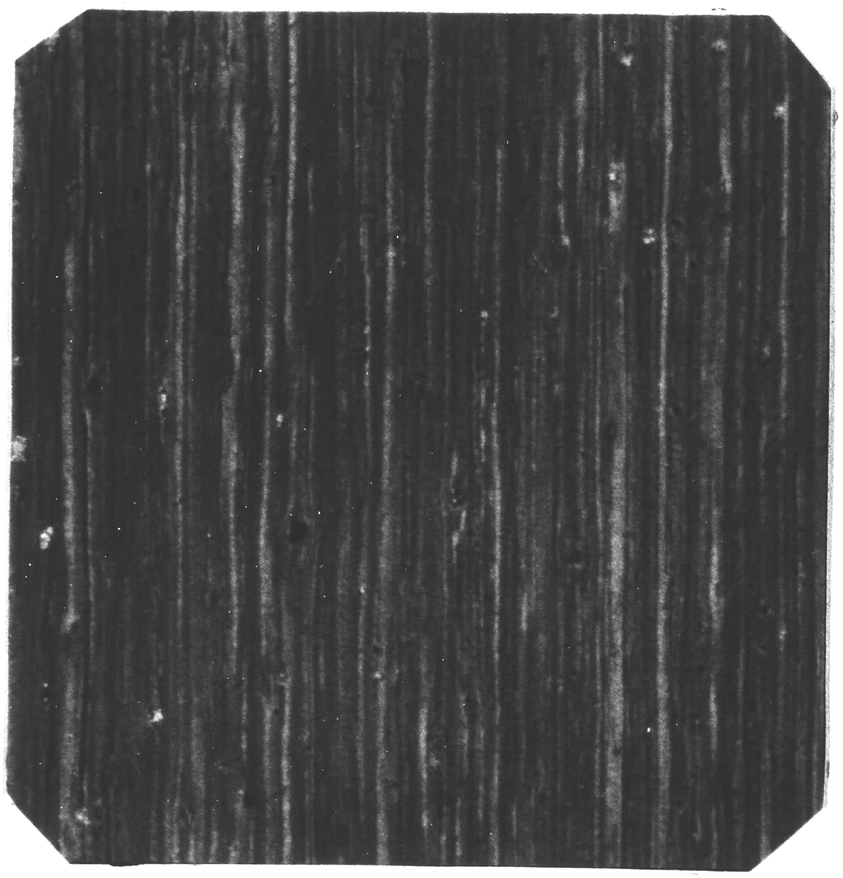

C. DRAWN

TRUE STRAIN - ϕ = 5.80 IN/IN

FINAL VELOCITY-V_f = 3.1 IN/SEC

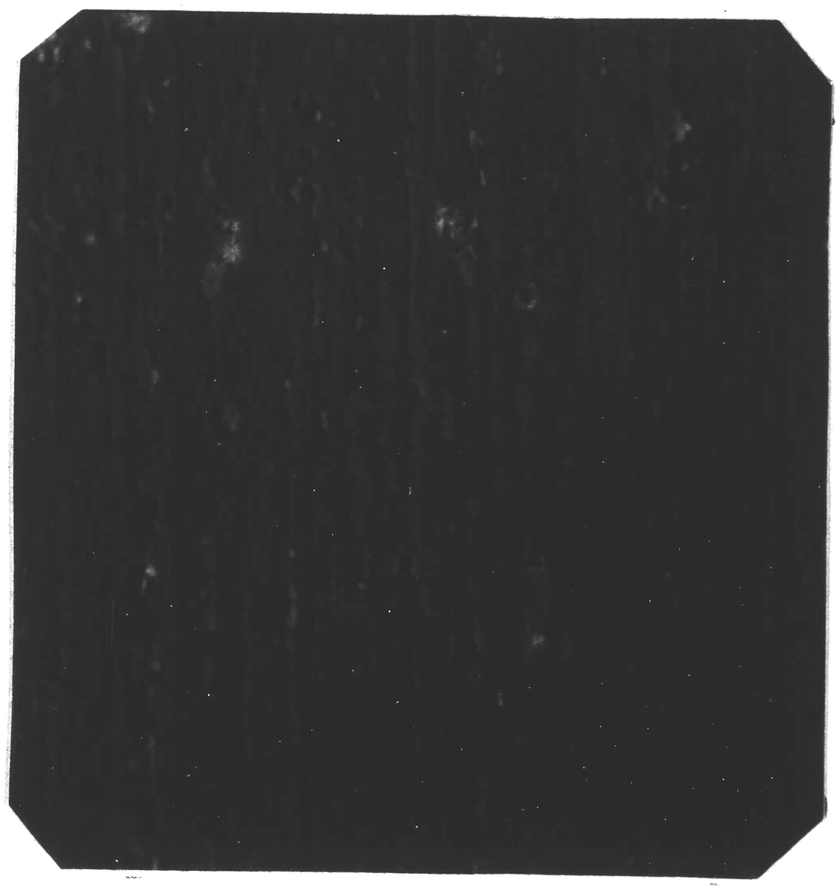

D. EXTRUDED

TRUE STRAIN- ϕ = 5.87 IN/IN

FINAL VELOCITY-V_f = 500 IN/SEC

FIGURE 12 - 500X PHOTOMICROGRAPHS E C ALUMINUM

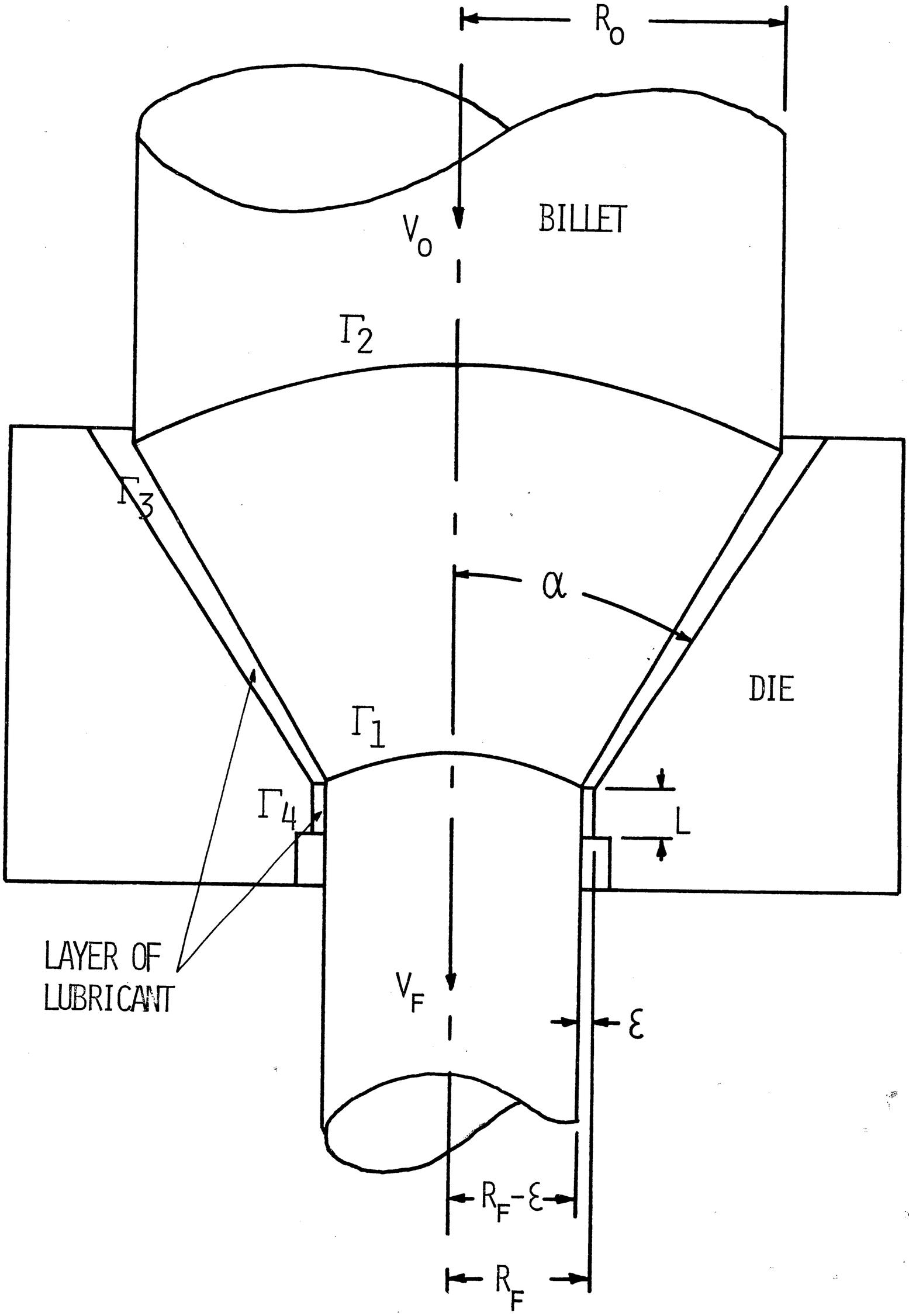

FIGURE 13 DIE AND EXTRUSION GEOMETRY

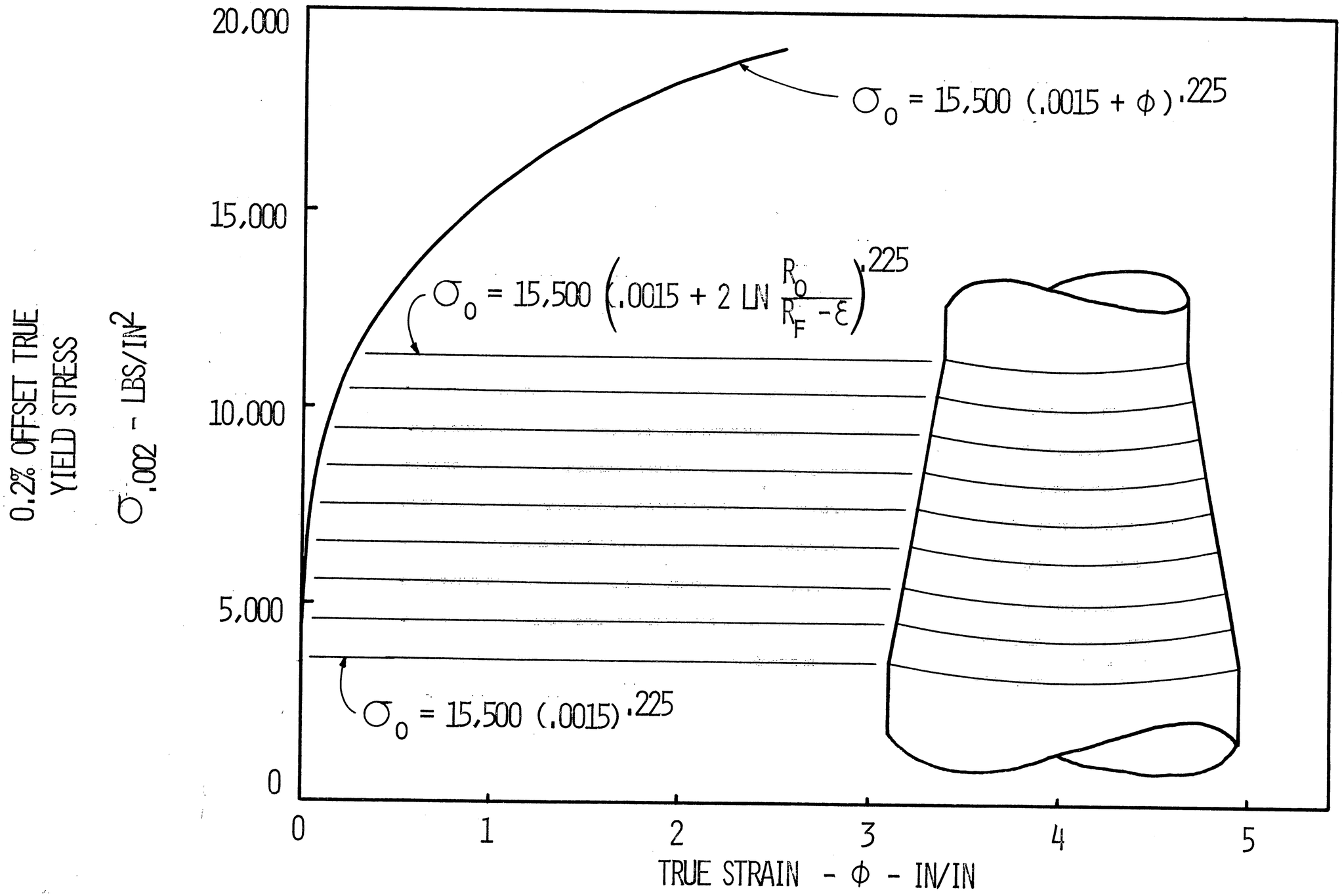

FIGURE 13.5 - INCREASE IN FLOW STRESS THROUGH DIE

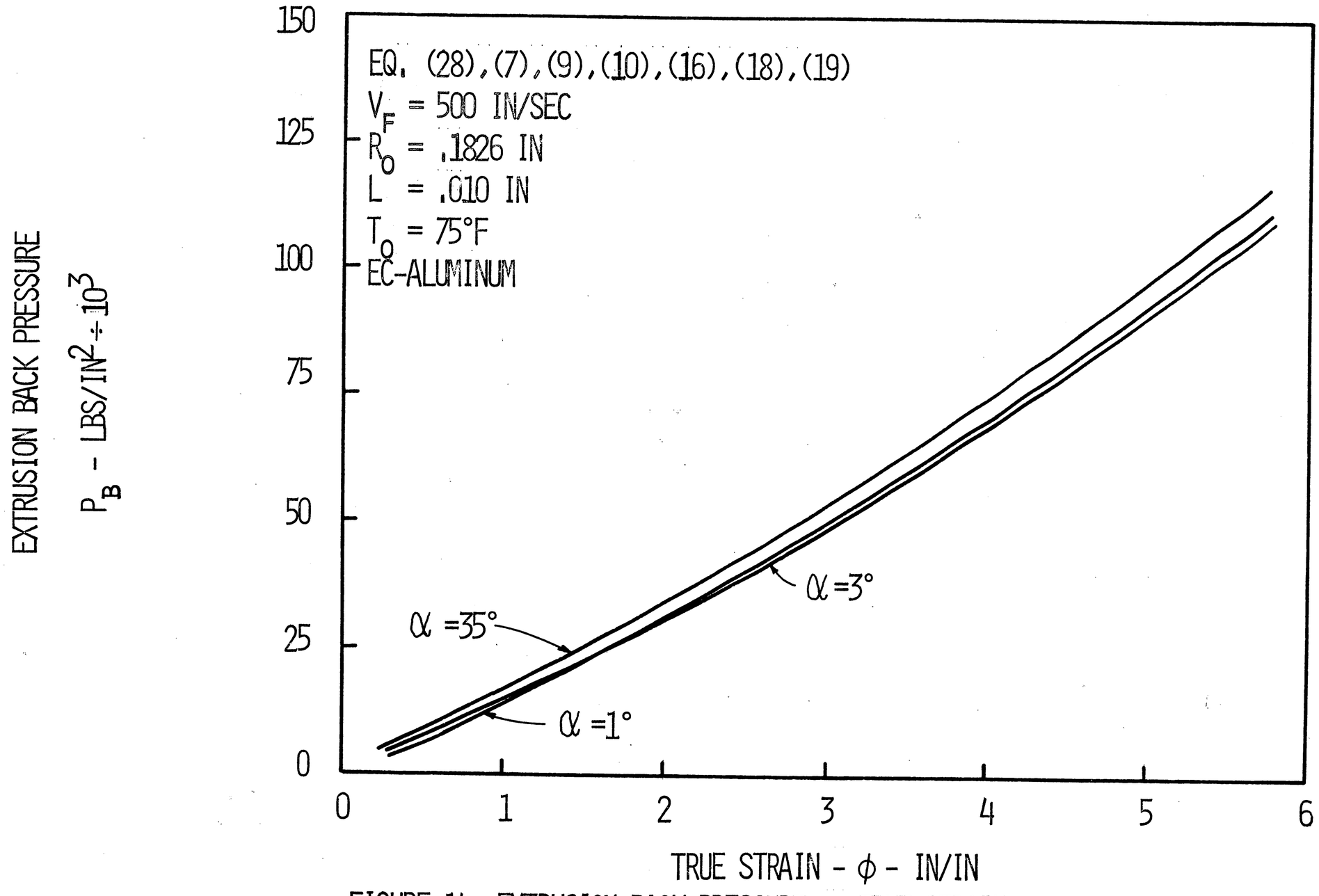

FIGURE 14 EXTRUSION BACK PRESSURE vs TRUE STRAIN

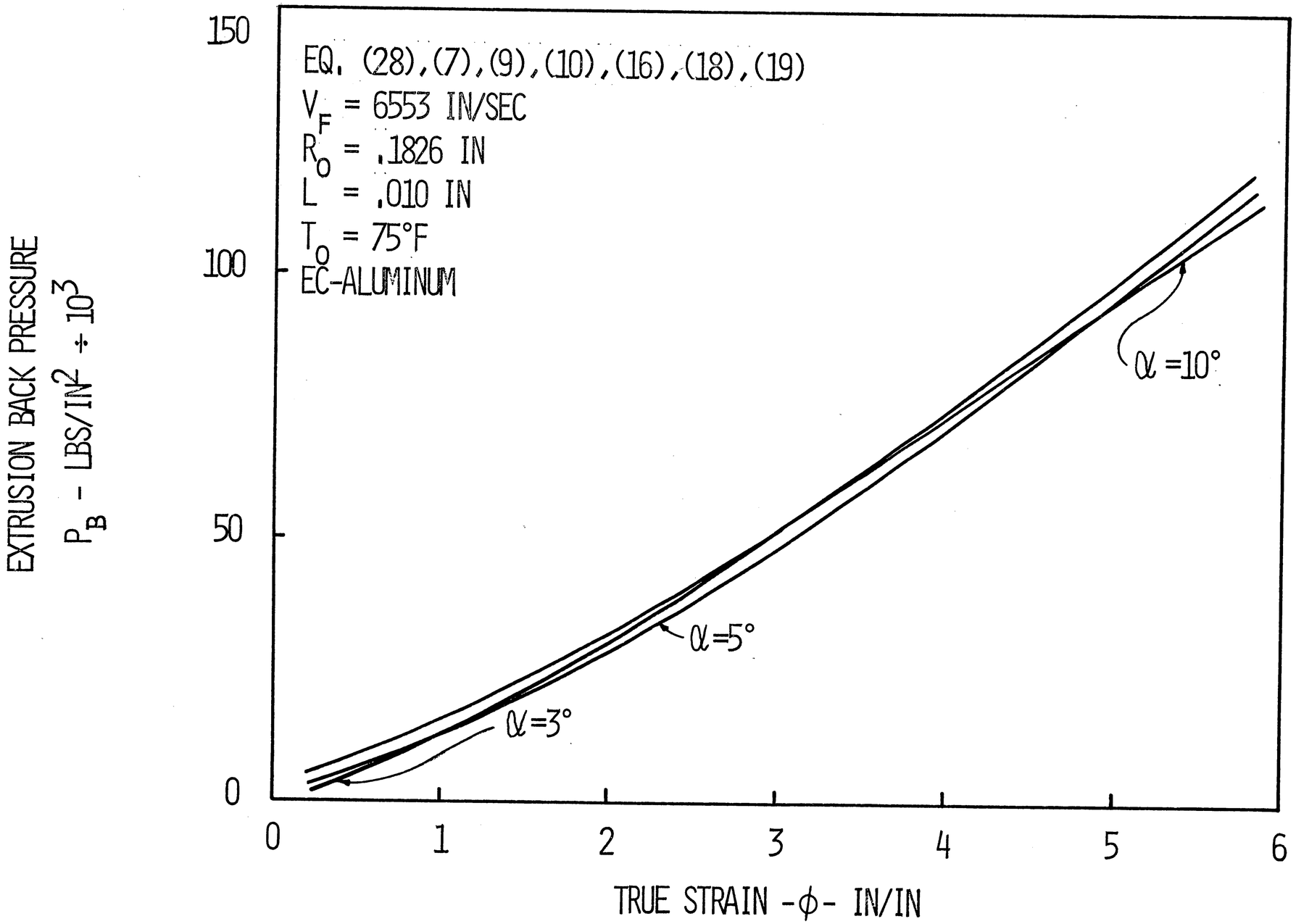

FIGURE 15 EFFECT OF TRUE STRAIN ON OPTIMUM DIE ANGLE

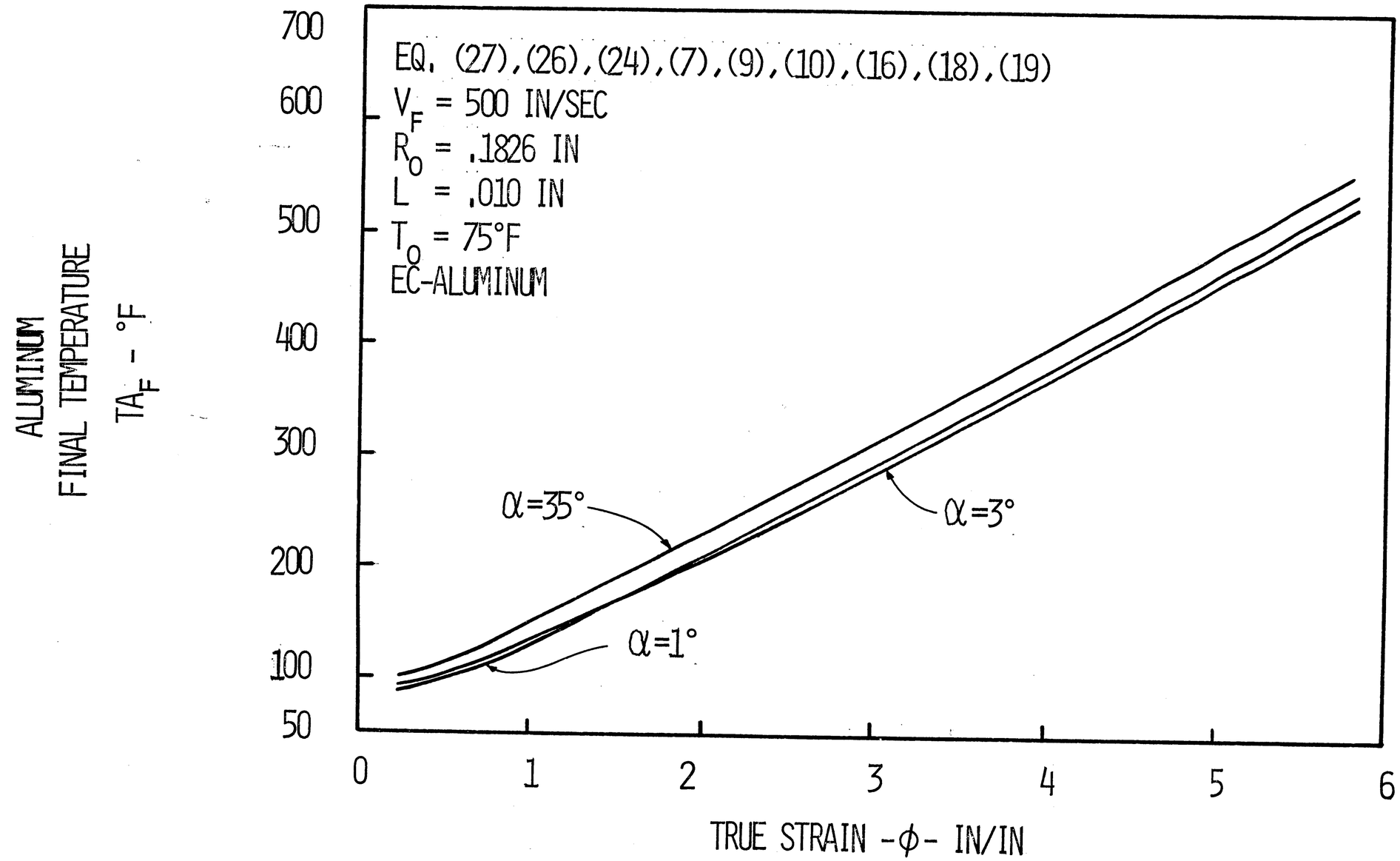

FIGURE 16 ALUMINUM FINAL TEMPERATURE
vs TRUE STRAIN

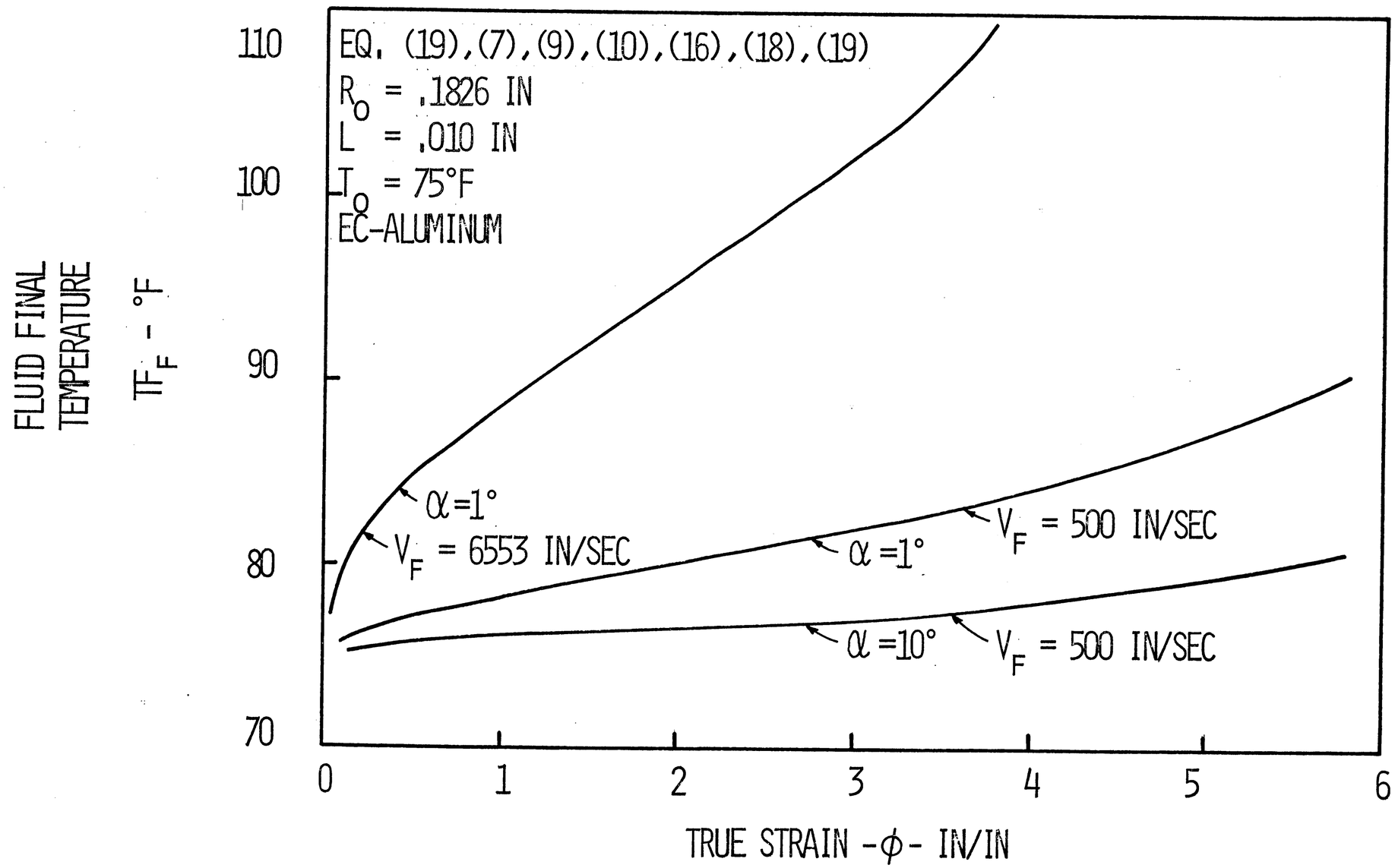

FIGURE 17 FLUID FINAL TEMPERATURE vs TRUE STRAIN

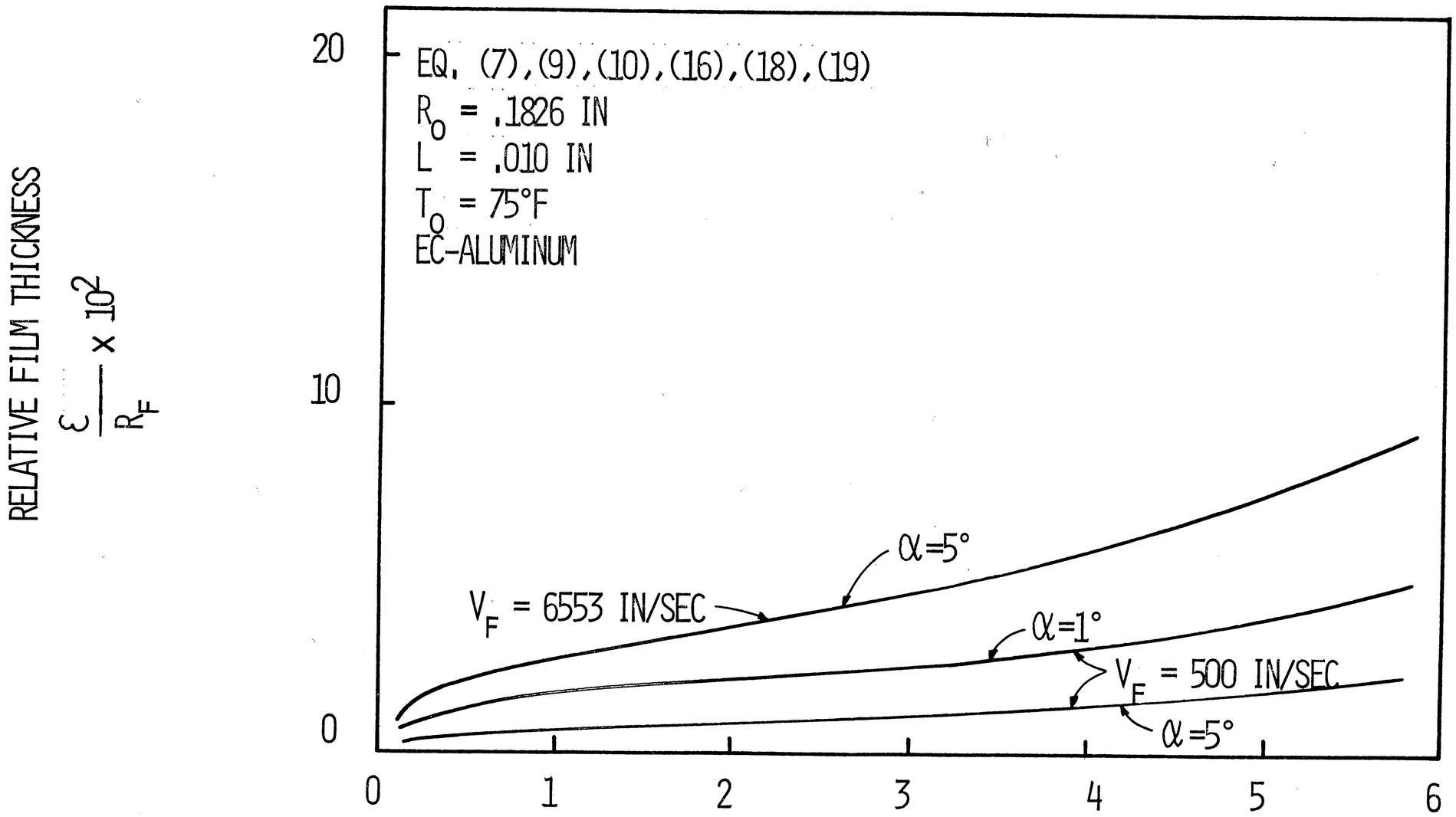

FIGURE 18 EFFECT OF TRUE STRAIN ON $\frac{\varepsilon}{R_F}$

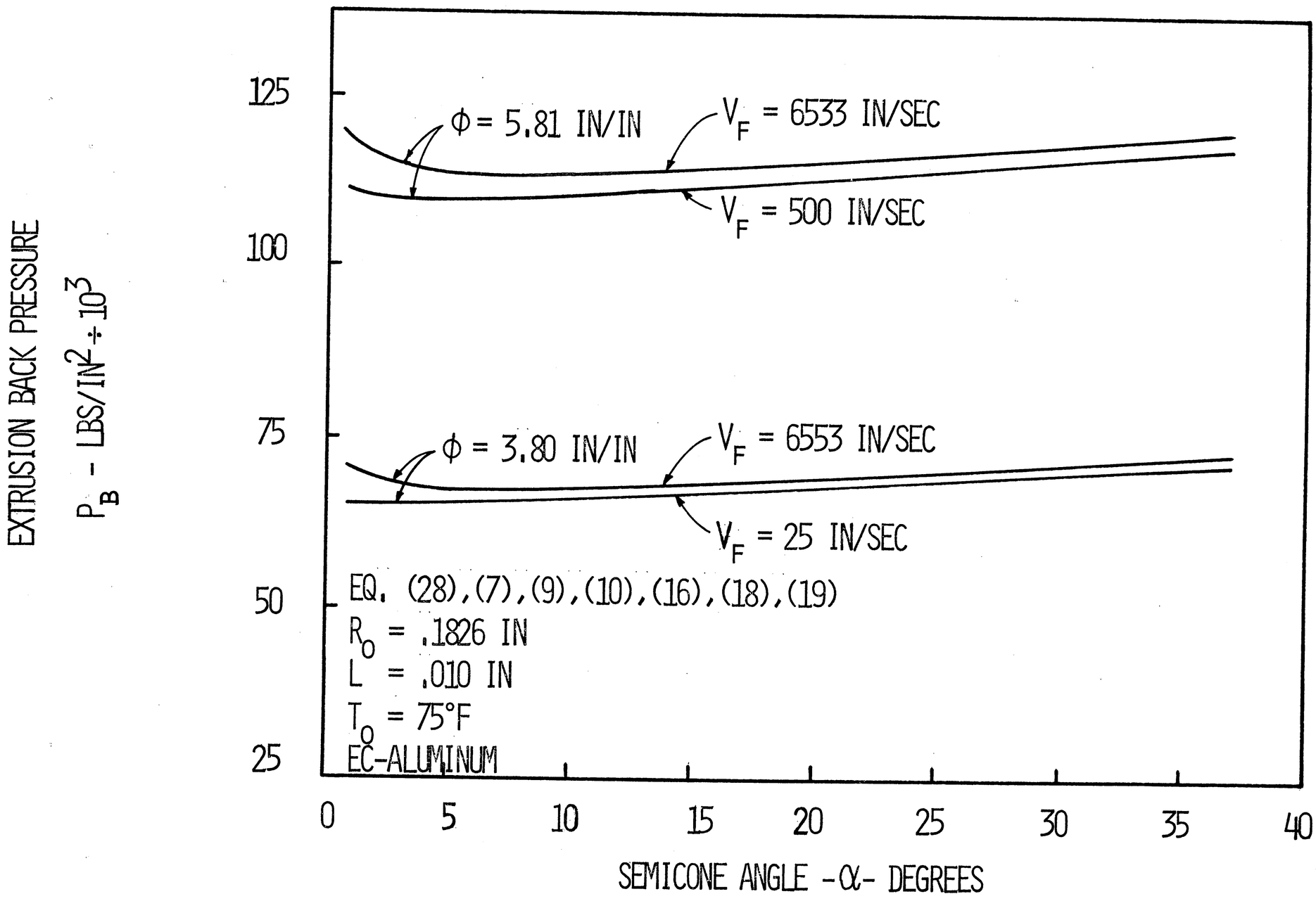

FIGURE 19 EXTRUSION BACK PRESSURE vs SEMICONE ANGLE

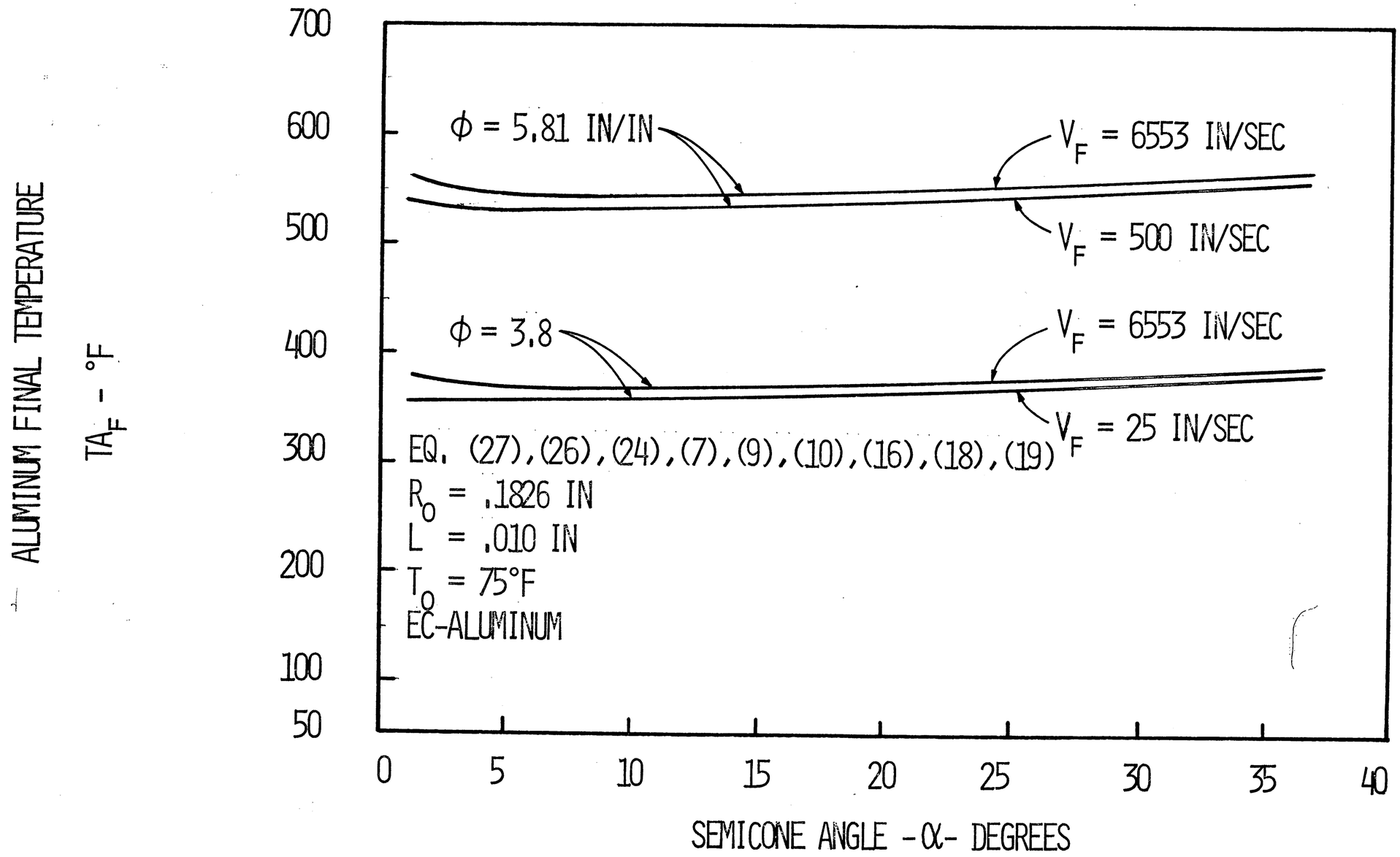

FIGURE 20 ALUMINUM FINAL TEMPERATURE vs SEMICONE ANGLE

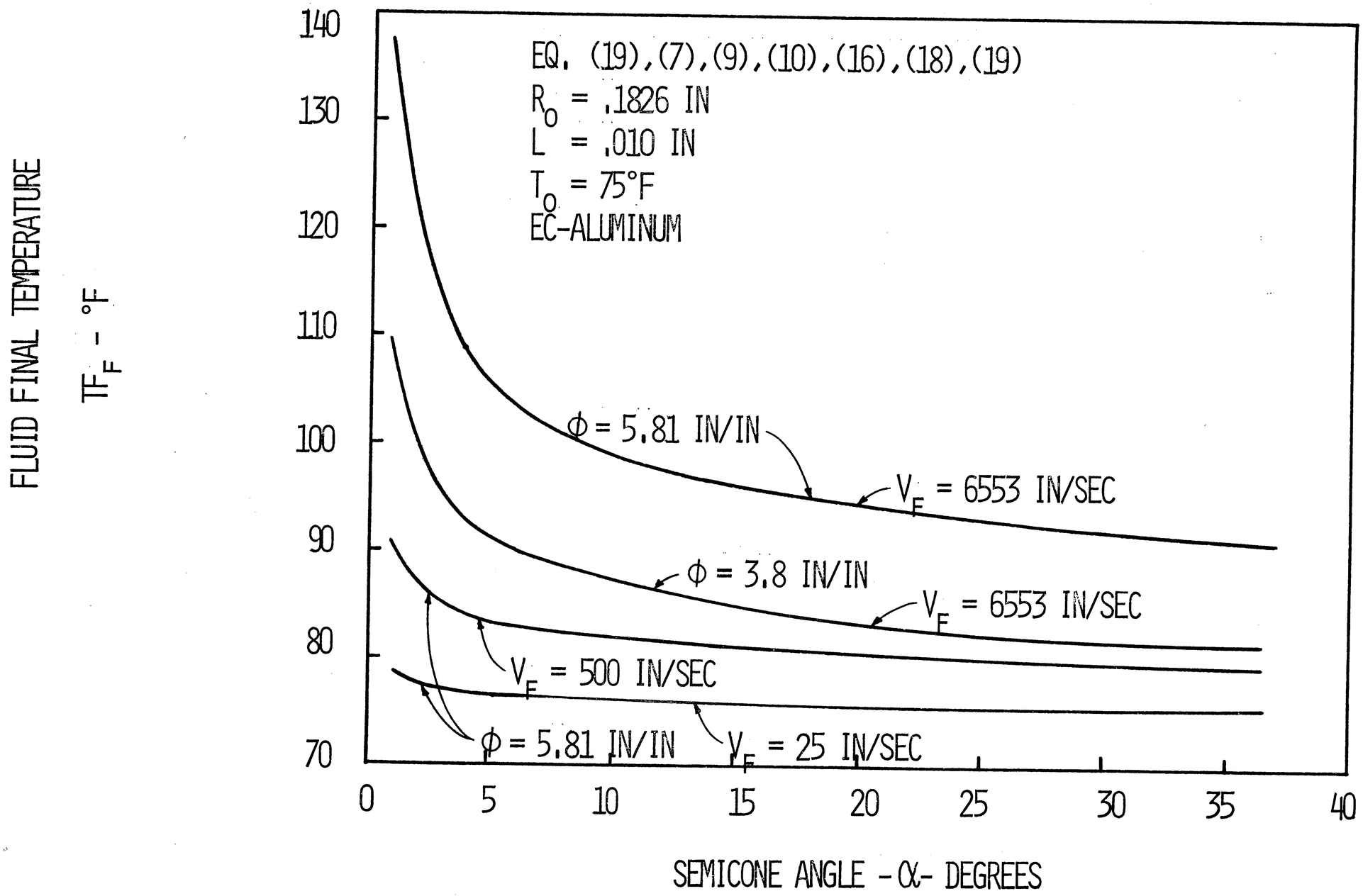

FIGURE 21 EFFECT OF SEMICONE ANGLE ON FLUID TEMPERATURE

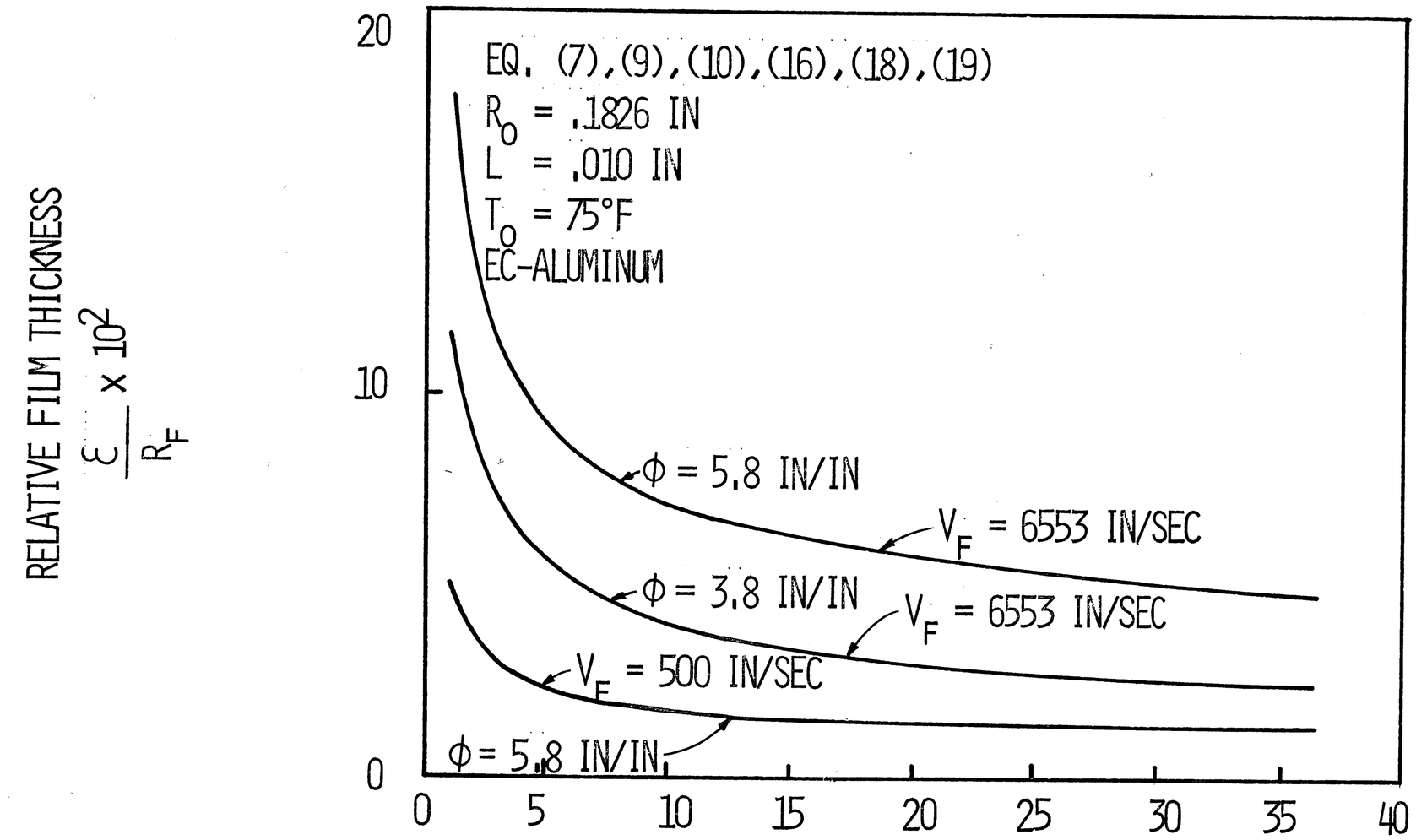

FIGURE 22 EFFECT OF SEMICONE ANGLE ON $\frac{\varepsilon}{R_F}$

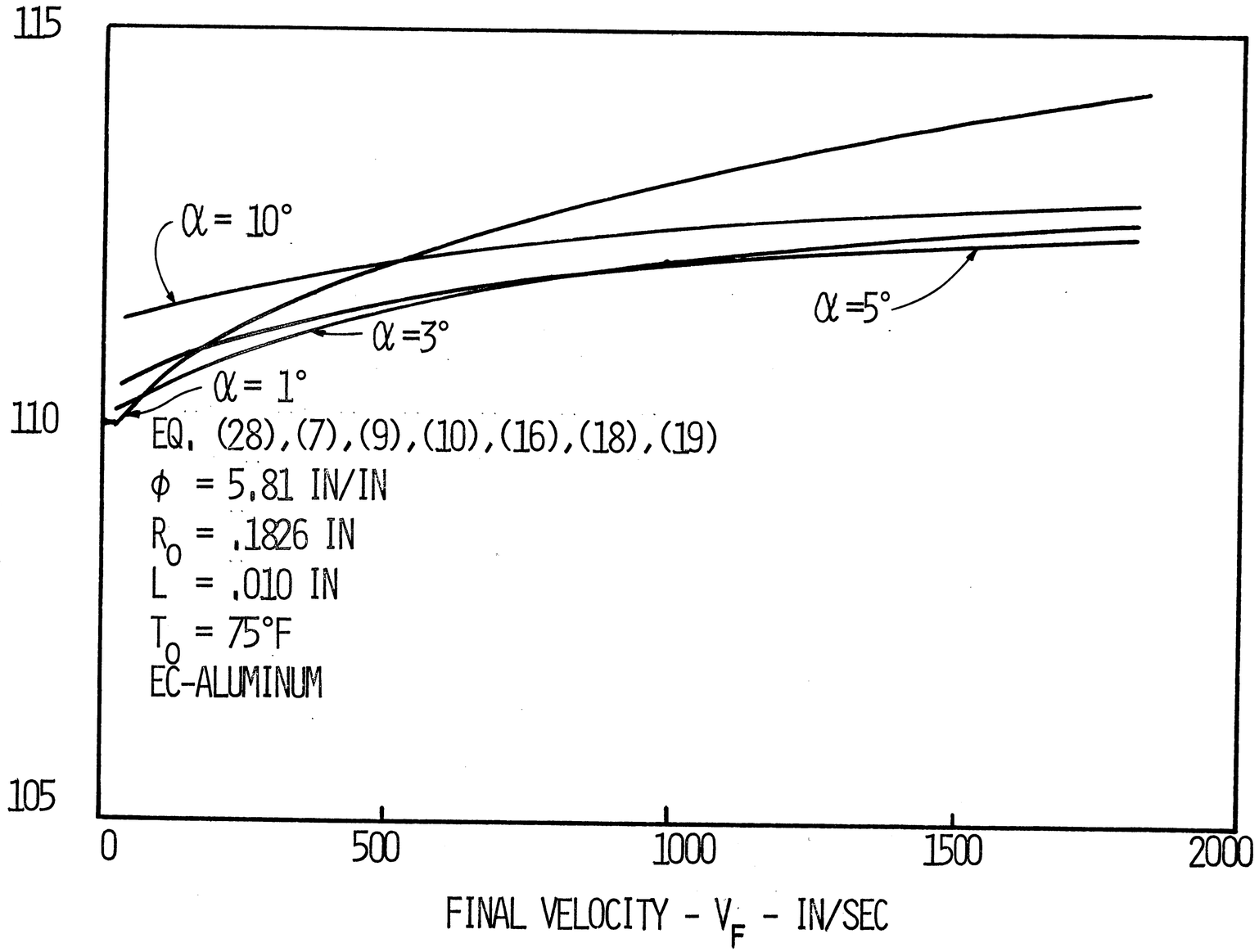

FIGURE 23 EFFECT OF VELOCITY ON OPTIMUM CONE ANGLE

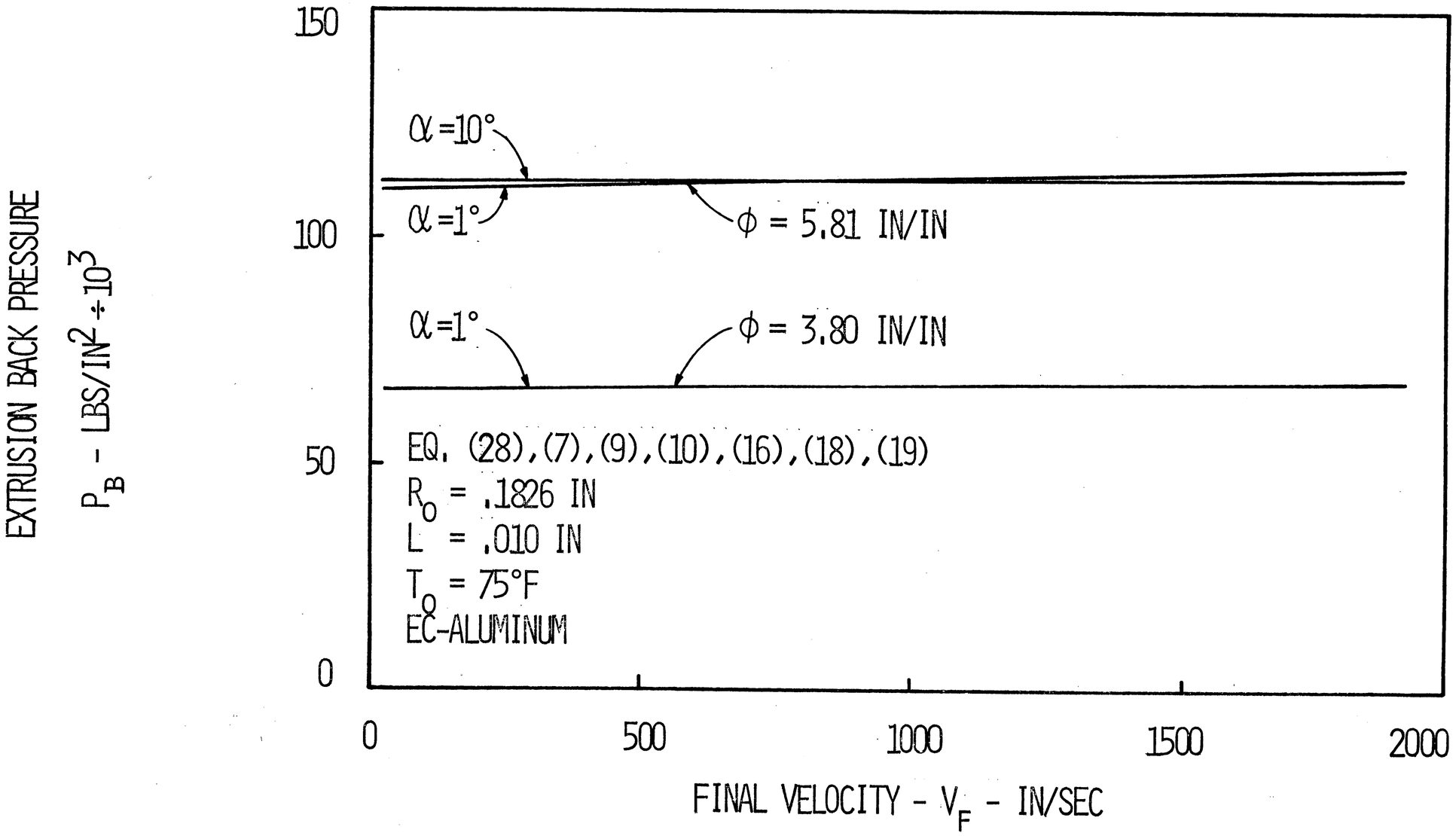

FIGURE 24 EXTRUSION BACK PRESSURE vs FINAL VELOCITY

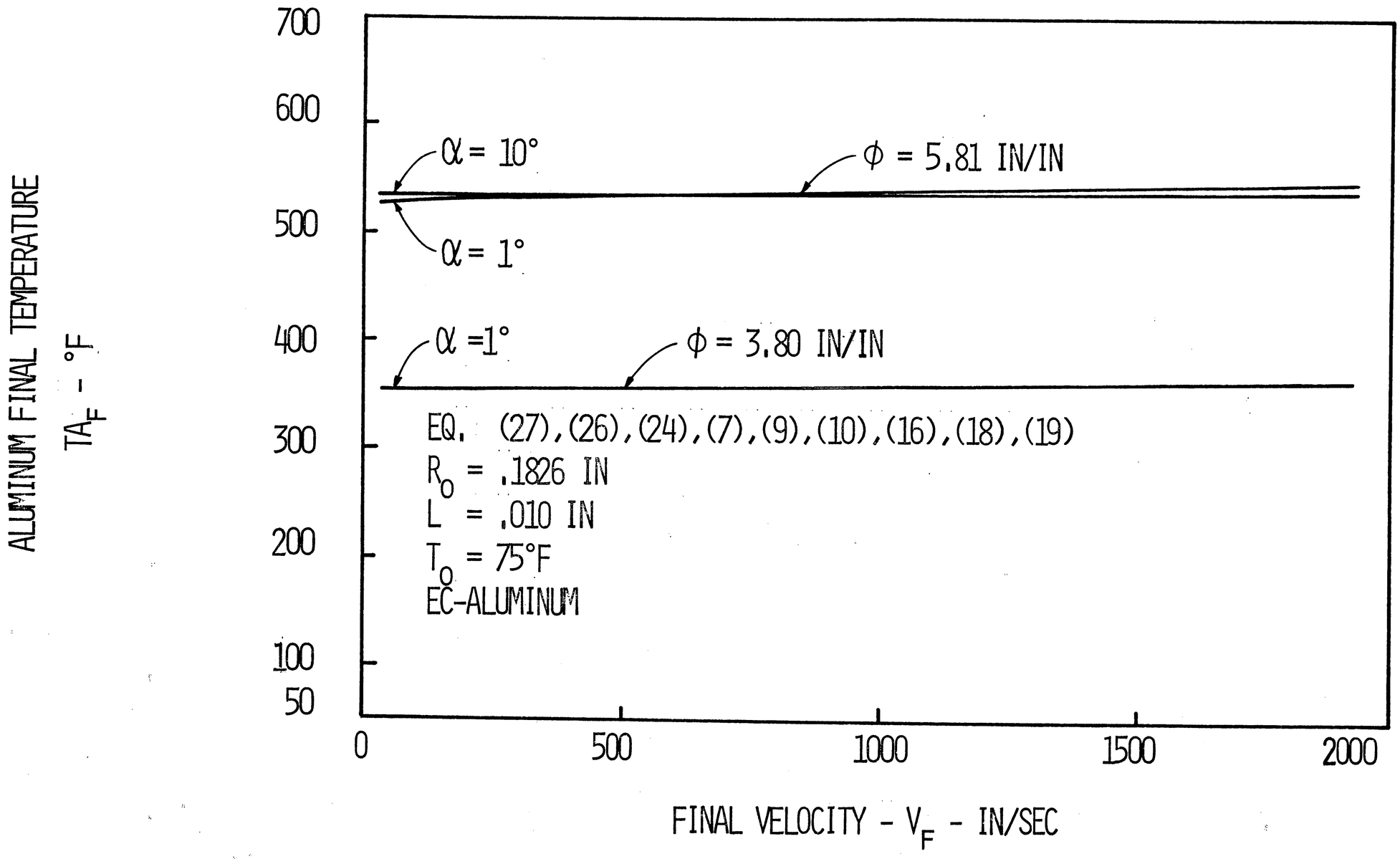

FIGURE 25 ALUMINUM FINAL TEMPERATURE vs FINAL VELOCITY

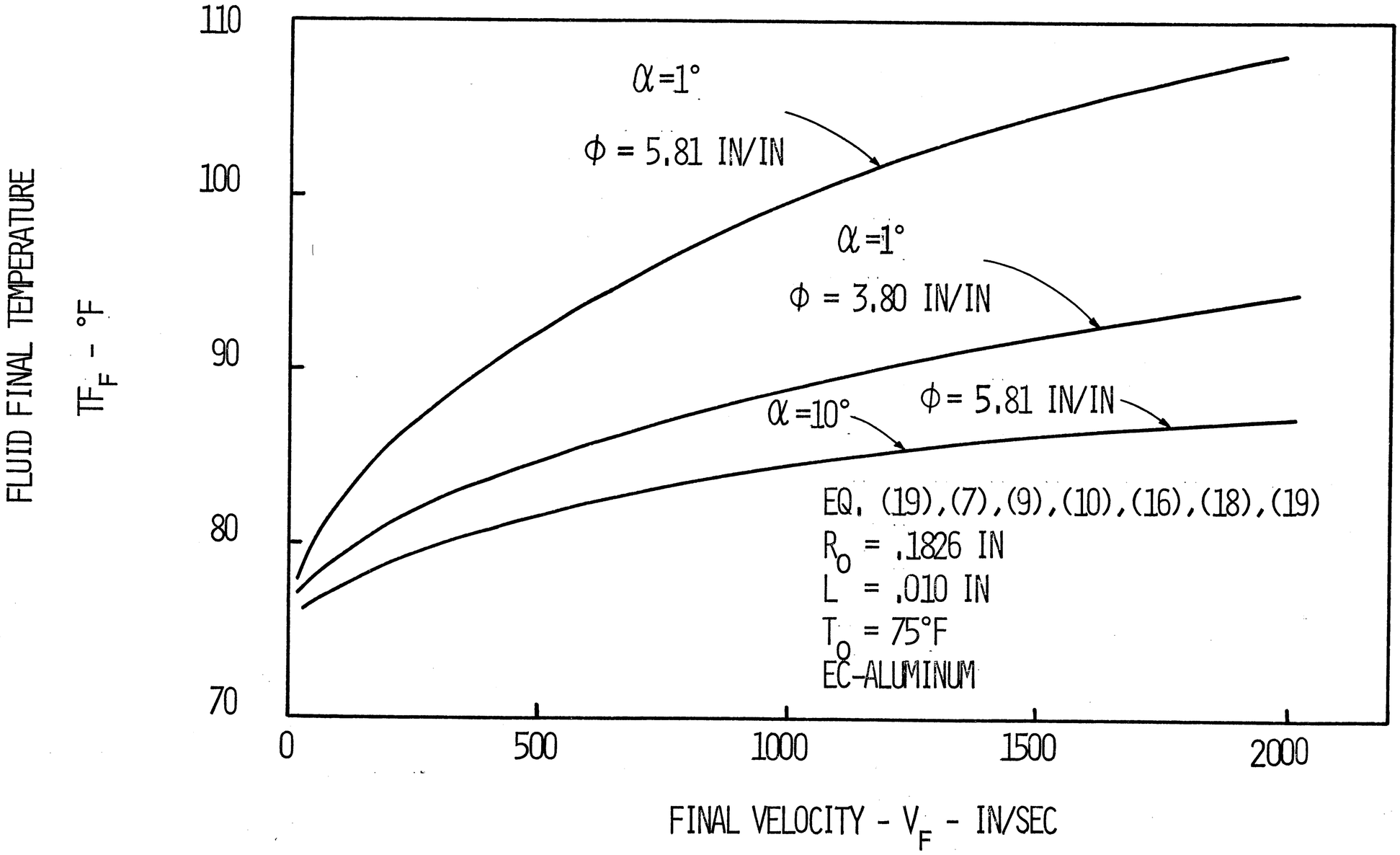

FIGURE 26 FLUID FINAL TEMPERATURE vs FINAL VELOCITY

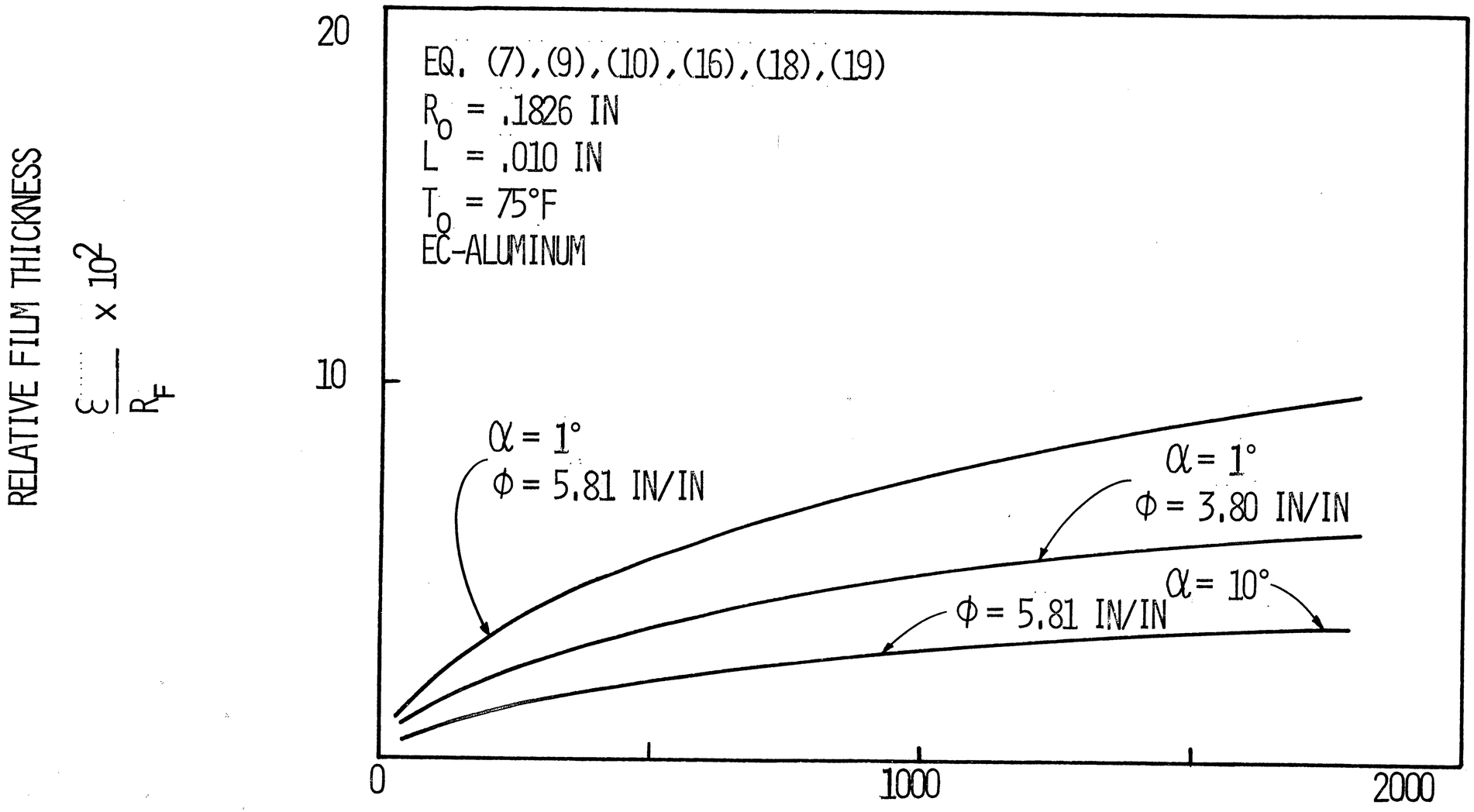

FIGURE 27 EFFECT OF FINAL VELOCITY ON $\frac{\varepsilon}{R_F}$

TABLE 1

HYDROSTATIC EXTRUSION TENSILE PROPERTIES
E C ALUMINUM

D_o = .3652 Inch Gage Length = 10 Inch Crosshead Speed = 0.1 Inch/Minute

Semicone Angle α (Degrees)	Final Diameter D_f (Inch)	True Strain By Extrusion ϕ (in/in)	Reduction In Area By Extrusion R.A. (%)	0.2% Offset True Yield Stress $\sigma_{.002}$ (lbs/in^2)	True Stress At Ultimate Load $\sigma_{Ult.}$ (lbs/in^2)	Elongation At Ultimate Load (%)	Elongation At Fracture (%)
10	.3245	.236	21.0	11499	12218	3.1	11.6
10	.3245	.236	21.0	11560	12272	3.4	9.6
10	.3245	.236	21.0	10965	11743	3.2	8.4
15	.3251	.232	20.8	11541	12151	2.3	6.6
15	.3251	.232	20.8	11481	12139	2.4	6.7
10	.2890	.468	37.4	13154	13962	2.3	5.9
10	.2890	.468	37.4	13307	14136	2.5	5.6
15	.2900	.461	36.9	12835	13612	2.2	4.4
15	.2900	.461	36.9	13367	14062	2.1	4.1
15	.2900	.461	36.9	13565	14311	2.2	4.7
10	.2575	.698	50.3	14258	15187	2.5	5.6
10	.2575	.698	50.3	14451	15230	2.7	4.4
10	.2575	.698	50.3	14008	14790	2.6	4.5
15	.2570	.702	50.5	14508	15509	2.4	5.5
15	.2570	.702	50.5	14082	15034	2.4	5.4
15	.2570	.702	50.5	14120	15147	2.3	6.3
15	.2570	.702	50.5	14663	15714	2.4	5.9

TABLE 1 (Cont'd)

HYDROSTATIC EXTRUSION TENSILE PROPERTIES
E C ALUMINUM

D_o = .3652 Inch Gage Length = 10 Inch Crosshead Speed = 0.1 Inch/Minute

Semicone Angle α (Degrees)	Final Diameter D_f (Inch)	True Strain By Extrusion ϕ (in/in)	Reduction In Area By Extrusion R.A. (%)	0.2% Offset True Yield Stress $\sigma_{.002}$ (lbs/in^2)	True Stress At Ultimate Load $\sigma_{Ult.}$ (lbs/in^2)	Elongation At Ultimate Load (%)	Elongation At Fracture (%)
10	.2297	.927	60.4	15329	16515	2.9	5.5
10	.2297	.927	60.4	15256	16409	3.0	5.8
10	.2297	.927	60.4	14311	15463	2.7	5.6
15	.2289	.934	60.7	15095	16088	2.5	5.6
15	.2289	.934	60.7	15070	15929	2.3	4.6
15	.2289	.934	60.7	15388	16331	2.3	4.7
20	.2385	.852	57.4	16917	17924	2.3	4.7
20	.2385	.852	57.4	16715	17780	2.4	4.8
15	.1148	2.31	90.1	19592	20789	1.5	2.5
15	.1148	2.31	90.1	19495	20809	1.6	2.5
15	.1148	2.31	90.1	17455	19129	-	-
20	.1163	2.29	89.9	18427	19674	-	-
20	.1163	2.29	89.9	20131	21530	1.6	2.2
20	.1163	2.29	89.9	19847	21141	1.6	2.2
15	.0530	3.86	97.9	14874	17139	1.4	1.5
15	.0530	3.86	97.9	15101	17399	1.3	1.4
15	.0530	3.86	97.9	16696	18813	1.2	1.4

TABLE 1 (Cont'd)

HYDROSTATIC EXTRUSION TENSILE PROPERTIES
E C ALUMINUM

D_o = .3652 Inch Gage Length = 10 Inch Crosshead Speed = 0.1 Inch/Minute

Semicone Angle α (Degrees)	Final Diameter D_f (Inch)	True Strain By Extrusion ϕ (in/in)	Reduction In Area By Extrusion R.A. (%)	0.2% Offset True Yield Stress $\sigma_{.002}$ (lbs/in^2)	True Stress At Ultimate Load $\sigma_{Ult.}$ (lbs/in^2)	Elongation At Ultimate Load (%)	Elongation At Fracture (%)
20	.0463	4.13	98.4	14065	15957	1.4	1.5
20	.0463	4.13	98.4	13587	15600	1.4	1.5
20	.0463	4.13	98.4	14602	15719	1.0	1.2
25	.0472	4.09	98.3	13877	15719	1.5	1.6
25	.0472	4.09	98.3	14854	17263	1.3	1.5
25	.0472	4.09	98.3	16571	17409	1.4	1.5
25	.0472	4.09	98.3	16824	18733	.8	1.3
25	.0472	4.09	98.3	14044	15326	.9	1.4
30	.0442	4.22	98.5	13798	15719	1.3	1.5
30	.0442	4.22	98.5	13929	14929	.9	1.1
30	.0442	4.22	98.5	15304	15848	.9	1.1
30	.0442	4.22	98.5	15370	17140	1.2	1.3
20	.0255	5.32	99.5	10390	11244	1.1	1.7
20	.0255	5.32	99.5	9780	10712	1.6	2.2
20	.0255	5.32	99.5	10685	11263	1.4	1.5
20	.0255	5.32	99.5	11097	11810	1.2	1.3
25	.0194	5.87	99.7	9331	9743	-	-
25	.0194	5.87	99.7	9568	9738	1.0	1.1

TABLE 1 (Cont'd)

HYDROSTATIC EXTRUSION TENSILE PROPERTIES
E C ALUMINUM

D_o = .3652 Inch Gage Length = 10 Inch Crosshead Speed = 0.1 Inch/Minute

Semicone Angle α (Degrees)	Final Diameter D_f (Inch)	True Strain By Extrusion ϕ (in/in)	Reduction In Area By Extrusion R.A. (%)	0.2% Offset True Yield Stress $\sigma_{.002}$ (lbs/in^2)	True Stress At Ultimate Load $\sigma_{Ult.}$ (lbs/in^2)	Elongation At Ultimate Load (%)	Elongation At Fracture (%)
25	.0194	5.87	99.7	9093	9399	1.0	1.1
25	.0194	5.87	99.7	9772	10104	0.9	1.1
25	.0194	5.87	99.7	9840	10097	0.8	.9

TABLE 2

AVERAGE RUNOUT PRESSURE AND VELOCITIES
HYDROSTATIC EXTRUDED E C ALUMINUM

D_o = .3652 Inch

Semicone Angle α (Degrees)	Final Diameter D_f (Inch)	True Strain ϕ (in/in)	Average Runout Pressure P_b (lb/in^2)	Initial Velocity v_o (in/sec)	Final Velocity v_f (in/sec)
10	.3245	.236	4,693	.17	.22
15	.3251	.232	5,656	.17	.21
10	.2890	.468	9,145	.17	.27
15	.2900	.461	9,145	.17	.27
10	.2575	.698	14,784	.17	.34
15	.2570	.702	13,638	.17	.34
10	.2297	.927	19,483	.17	.43
15	.2289	.934	19,414	.17	.43
20	.2385	.852	18,040	.17	.40
15	.1148	2.31	52,144	.17	1.72
20	.1163	2.29	54,551	.17	1.67
15	.0530	3.86	89,849	.84	39.69
20	.0463	4.13	96,266	.84	51.79
25	.0472	4.09	97,871	.84	50.05
30	.0442	4.22	101,882	.84	57.07
20	.0255	5.32	129,960	1.41	286.95
25	.0194	5.87	144,400	1.41	499.66

TABLE 3

DRAWN TENSILE PROPERTIES
E C ALUMINUM

D_o = .3652 Inch Gage Length = 10 Inch Crosshead Speed = 0.1 Inch/Minute

Final Diameter D_f (Inch)	True Strain By Drawing ϕ (in/in)	Reduction In Area By Drawing R.A. (%)	0.2% Offset True Yield Stress $\sigma_{.002}$ (lbs/in^2)	True Stress At Ultimate Load σ_{Ult} (lbs/in^2)	Elongation At Ultimate Load (%)	Elongation At Fracture (%)
.3241	.238	21.2	11247	12090	3.9	9.2
.3241	.238	21.2	10724	12010	3.8	7.3
.3241	.238	21.2	11308	12034	3.2	8.5
.2914	.451	36.3	12426	13327	3.4	6.6
.2914	.451	36.3	12441	13196	3.3	7.7
.2914	.451	36.3	12561	13345	3.4	7.2
.2552	.716	51.2	14124	14832	3.2	6.8
.2552	.716	51.2	13908	14683	3.3	5.9
.2552	.716	51.2	13967	14841	3.3	7.1
.2269	.951	61.4	15213	16039	2.6	5.6
.2269	.951	61.4	15139	16003	2.6	6.4
.2269	.951	61.4	15437	16190	2.6	6.2
.1130	2.35	90.4	19420	20632	1.9	3.9
.1130	2.35	90.4	19120	20423	1.9	4.6
.1130	2.35	90.4	19220	20445	2.5	4.7
.0631	3.51	97.0	18403	22296	2.7	6.7
.0631	3.51	97.0	18120	22093	2.4	6.7

TABLE 3 (Cont'd)

DRAWN TENSILE PROPERTIES
E C ALUMINUM

D_o = .3652 Inch Gage Length = 10 Inch Crosshead Speed = 0.1 Inch/Minute

Final Diameter D_f (Inch)	True Strain By Drawing ϕ (in/in)	Reduction In Area By Drawing R.A. (%)	0.2% Offset True Yield Stress $\sigma_{.002}$ (lbs/in^2)	True Stress At Ultimate Load σ_{Ult} (lbs/in^2)	Elongation At Ultimate Load (%)	Elongation At Fracture (%)
.0569	3.72	97.6	18104	21604	2.5	5.2
.0569	3.72	97.6	19065	21843	2.4	5.5
.0569	3.72	97.6	19848	22171	2.3	5.8
.0569	3.72	97.6	18052	21785	2.1	5.2
.0569	3.72	97.6	19500	22005	2.3	5.3
.0504	3.96	98.1	20085	22817	2.2	5.4
.0504	3.96	98.1	20090	22738	2.4	5.3
.0504	3.96	98.1	19086	22153	2.3	4.8
.0451	4.18	98.5	20231	24095	2.1	2.6
.0451	4.18	98.5	20231	24157	2.2	3.1
.0451	4.18	98.5	19556	22272	1.7	3.3
.0451	4.18	98.5	20321	22975	1.7	2.8
.0451	4.18	98.5	20043	22375	1.5	2.7
.0451	4.18	98.5	20321	22579	2.6	5.6
.0451	4.18	98.5	20188	22667	2.3	5.3
.0402	4.41	98.8	20060	22550	1.4	2.7
.0402	4.41	98.8	20052	22513	1.6	3.0

TABLE 3 (Cont'd)

DRAWN TENSILE PROPERTIES
E C ALUMINUM

D_o = .3652 Inch Gage Length = 10 Inch Crosshead Speed = 0.1 Inch/Minute

Final Diameter D_f (Inch)	True Strain By Drawing ϕ (in/in)	Reduction In Area By Drawing R.A. (%)	0.2% Offset True Yield Stress $\sigma_{.002}$ (lbs/in^2)	True Stress At Ultimate Load σ_{Ult} (lbs/in^2)	Elongation At Ultimate Load (%)	Elongation At Fracture (%)
.0353	4.67	99.1	21269	23460	1.1	2.0
.0353	4.67	99.1	21495	24453	1.5	2.5
.0353	4.67	99.1	21721	24213	1.4	2.4
.0317	4.89	99.2	21463	23402	1.2	2.0
.0317	4.89	99.2	22024	24323	1.3	2.0
.0317	4.89	99.2	22356	24566	1.3	2.1
.0317	4.89	99.2	21323	23453	1.2	2.0
.0282	5.12	99.4	22687	24684	1.0	2.0
.0282	5.12	99.4	22687	24884	1.1	2.0
.0282	5.12	99.4	22156	23642	1.0	1.9
.0249	5.37	99.5	23657	26136	1.3	1.8
.0249	5.37	99.5	22748	25164	1.0	1.8
.0249	5.37	99.5	22272	24474	1.0	1.9
.0224	5.58	99.6	23319	23825	0.9	1.5
.0224	5.58	99.6	22859	25424	1.0	1.8
.0224	5.58	99.6	22476	23707	0.9	1.6
.0201	5.80	99.7	24913	27953	1.4	2.1
.0201	5.80	99.7	24215	24785	0.7	0.8

TABLE 3 (Cont'd)

DRAWN TENSILE PROPERTIES
E C ALUMINUM

D_o = .3652 Inch Gage Length = 10 Inch Crosshead Speed = 0.1 Inch/Minute

Final Diameter D_f (Inch)	True Strain By Drawing ϕ (in/in)	Reduction In Area By Drawing R.A. (%)	0.2% Offset True Yield Stress $\sigma_{.002}$ (lbs/in^2)	True Stress At Ultimate Load σ_{Ult} (lbs/in^2)	Elongation At Ultimate Load (%)	Elongation At Fracture (%)
.0201	5.80	99.7	24850	25560	0.8	1.0
.0201	5.80	99.7	24564	25330	0.7	1.0
.0201	5.80	99.7	24152	24915	0.9	1.1
.0201	5.80	99.7	24437	26065	0.9	1.2
.0201	5.80	99.7	24977	28081	1.5	1.8

TABLE 4

ANNEALED TENSILE PROPERTIES
EC ALUMINUM

D_o = .3652 inch Gage length = 10 inch Crosshead speed = 0.1 inch/minute

0.2% Offset True Yield Stress $\sigma_{.002}$ (lbs/in^2)	True Stress At Ultimate Load $\sigma_{ult.}$ (lbs/in^2)	Elongation At Ultimate Load (%)	Elongation At Fracture (%)
3789	11562	28.3	44.1
3588	11329	27.3	40.6
3445	11159	25.8	42.2
3531	11303	27.6	42.8
3541	11324	27.5	37.8

TABLE 5

DENSITY DATA
DIETHYLENE GLYCOL MONOETHYL ETHER

Temp (^{o}C)	Density ($GM/_{CC}$)
20.4	1.03145
20.5	1.03116
21.0	1.03076
21.7	1.03000
22.2	1.02985
23.0	1.02926

TABLE 6

DENSITY DATA - 22°C
HYDROSTATIC EXTRUDED E C ALUMINUM

True Strain ϕ in/in	Density D ($GM/_{CC}$)	Relative Density $\frac{D_\phi}{D_{\phi=o}}$	Density D ($GM/_{CC}$)	Relative Density $\frac{D_\phi}{D_{\phi=o}}$
	Series No. 1		Series No. 2	
-0-	2.69508	1.0	2.69507	1.0
.236	2.69541	1.00012	2.69502	.99998
.468	2.69561	1.00020	2.69549	1.00016
.702	2.69583	1.00028	2.69555	1.00018
.934	2.69573	1.00024		
	Series No. 3		Series No. 4	
-0-	2.69495	1.0	2.69347	1.0
.236	2.69501	1.00002	2.69397	1.00019
.468	2.69513	1.00007	2.69453	1.00039
.702	2.69521	1.00010	2.69450	1.00038
.934	2.69525	1.00011	2.69497	1.00056
	Series No. 5		Series No. 6	
-0-	2.69356	1.0	2.69362	1.0
.236	2.69366	1.00004	2.69405	1.00016
.468	2.69437	1.00026	2.69436	1.00028
.702	2.69450	1.00035	2.69447	1.00032
.934	2.69473	1.00043	2.69482	1.00045
	Series No. 7		Series No. 8	
-0-	2.69547	1.0	2.69516	1.0
.236	2.69539	.99997	2.69573	1.00021
.468	2.69555	1.00003	2.69561	1.00017
.702	2.69539	.99997	2.69539	1.00009
.934	2.69544	.99999		

TABLE 6 (Cont'd)

DENSITY DATA - 22°C
HYDROSTATIC EXTRUDED E C ALUMINUM

True Strain ϕ in/in	Density D ($GM/_{CC}$)	Relative Density $\frac{D_\phi}{D_{\phi=o}}$	Density D ($GM/_{CC}$)	Relative Density $\frac{D_\phi}{D_{\phi=o}}$
	Series No. 9		Series No. 10	
-0-	2.69542	1.0	2.72067	1.0
.236	2.69571	1.00011	2.72075	1.00003
.468	2.69550	1.00003	2.72087	1.00007
.702	2.69543	1.00000	2.72117	1.00018
.934	2.69558	1.00006	2.72084	1.00006
2.31			2.72213	1.00054
4.13			2.72589	1.00192
	Series No. 11		Series No. 12	
-0-	2.72108	1.0	2.72331	1.0
.236	2.72117	1.00003	2.72343	1.00004
.468	2.72099	.99997	2.72339	1.00003
.702	2.72165	1.00021	2.72345	1.00005
.934	2.72162	1.00020	2.72349	1.00007
2.31	2.72287	1.00066	2.72456	1.00046
4.13	2.72183	1.00028	2.72311	.99993

TABLE 7

DENSITY DATA - 22°C
DRAWN E C ALUMINUM

True Strain ϕ in/in	Density D (GM/CC)	Relative Density $D_\phi / D_{\phi=o}$	Density D (GM/CC)	Relative Density $D_\phi / D_{\phi=o}$
	Series No. 1		Series No. 2	
-0-	2.69684	1.0	2.69666	1.0
.238	2.69685	1.0	2.69654	.99996
.451	2.69716	1.00012	2.69702	1.00013
.716	2.69706	1.00008	2.69703	1.00014
.951	2.69676	.99997	2.69687	1.00008
	Series No. 3		Series No. 4	
-0-	2.69683	1.0	2.69716	1.0
.238	2.69691	1.00003	2.69677	.99986
.451	2.69685	1.00001	2.69712	.99999
.716	2.69680	.99999	2.69682	.99987
.951	2.69673	.99996	2.69683	.99988
	Series No. 5		Series No. 6	
-0-	2.69625	1.0	2.69601	1.0
.238	2.69648	1.00009	2.69633	1.00012
.451	2.69653	1.00010	2.69651	1.00019
.716	2.69660	1.00013	2.69653	1.00019
.951	2.69611	.99995	2.69614	1.00005
	Series No. 7		Series No. 8	
-0-	2.69552	1.0	2.69526	1.0
.238	2.69548	.99999	2.69545	1.00007
.451	2.69564	1.00005	2.69558	1.00012
.716	2.69578	1.00010	2.69526	1.0
.951	2.69577	1.00009	2.69534	1.00003

TABLE 7 (Cont'd)

DENSITY DATA - 22°C
DRAWN E C ALUMINUM

True Strain ϕ in/in	Density D (GM/CC)	Relative Density $D_\phi / D\phi=o$	Density D (GM/CC)	Relative Density $D_\phi / D\phi=o$
	Series No. 9		Series No. 10	
-0-	2.69514	1.0	2.72218	1.0
.238	2.69517	1.00001	2.72142	.99972
.451	2.69518	1.00002	2.72162	.99979
.716	2.69615	1.00038	2.72177	.99985
.951	2.69624	1.00041	2.72222	1.00002
2.35			2.72221	1.00001
4.18			2.72374	1.00009
	Series No. 11		Series No. 12	
-0-	2.72372	1.0	2.72240	1.0
.238	2.72342	.99989	2.72244	1.00002
.451	2.72361	.99996	2.72254	1.00005
.716	2.72330	.99985	2.72243	1.00001
.951	2.72310	.99977	2.72244	1.00002
2.35	2.72283	.99967	2.72323	1.00031
4.18	2.72411	.99993	2.72343	1.00023

TABLE 8

AVERAGE RELATIVE DENSITY
E C ALUMINUM

True Strain ϕ in/in	Average Relative Density $\frac{\sum_{o}^{n} \frac{D_\phi}{D_{\phi=o}}}{n}$
HYDROSTATIC EXTRUDED	
-0-	1.0
.236	1.00008
.468	1.00014
.702	1.00018
.934	1.00022
2.31	1.00055
4.13	1.00071
DRAWN	
-0-	1.0
.238	.99998
.451	1.00004
.716	1.00005
.951	1.00002
2.35	.99999
4.18	1.00008

APPENDIX I

Background

One of the early references to hydrostatic extrusion[24] described the process as a method of ". . . propelling metal rods, bars, tubes, tubular articles, plates and wires through dies . . . from closed vessels directly by the contact and pressure of a liquid in motion under a great degree of pressure . . .". Other investigators, Bridgman[3,4], Beresnev, Bulychev, Ryabinin, et al[5,25,26], Pugh[27,28] and others have done considerable work in the field and have made various proposals of reasons for the improved properties of hydrostatically extruded material. Some of the factors (not necessarily independent) which are considered to have an effect on properties are outlined below.

1. Microstructural Damage
2. Preferred Orientation
3. Dislocations

These factors will be considered in the following sections:

Microstructural Damage

Several investigators have discussed the reason for increased ductility under pressure and the improved properties after deformation as being associated with the suppression of crack and void nucleation and/or growth as a result of this pressure. Bridgman[3,4] states in a qualitative way that increased ductility and tensile strength are a result of the decreasing "damage" done by a given deformation under increased hydrostatic pressure. Bulychev et al[25]

observed that pores and cracks visable in the metal under the optical microscope may be closed during plastic deformation under high hydrostatic pressure. Beresnev et al[5] deformed copper with and without artificially induced pores and cracks, both by drawing and hydrostatic extrusion. The yield and tensile strengths of the hydrostatically extruded specimens are never less than the drawn. In addition, the yield and tensile strengths of the specimens with defects approached the values of those without defects, with deformation, indicating that the pores or cracks had been reduced. However, at higher deformations the yield and tensile strengths of the wire drawn specimens fell rapidly, indicating that the stress state was no longer capable of suppressing damage. Density measurements of specimens with pores and cracks showed that the density increased much faster with deformation by hydrostatic extrusion than by drawing and at higher deformations the density of drawn specimens began to decrease. The investigations of Ryabinin[26] show that these micro-defects could not be eliminated under a pressure of 100,000 kg/cm^2 alone, but with the proper plastic deformation, and the pressure, the pores and cracks diminished.

The work of Coffin and Rogers[7,15] involving strip drawing under various levels of hydrostatic pressure has shown a relationship between the resultant hydrostatic stress, as determined by the slip-line field analysis, and the structural damage as determined by metallographic examination, density changes and the reduction limits of the sheet at various pressures. Avitzur[6,11,29] discusses

the affect of the mean pressure induced in the process on the resultant density and mechanical properties of the material. The importance of die angle, reduction, friction and preferred orientation are also pointed out. Uy, Nolan and Davidson [30], Bobrowsky, Stack and Austen[31], Gelles[8], Austen, Kaklow and Rozovsky[32] and others all discuss the importance of the hydrostatic compressive stress on the stress-state-sensitive mechanisms of plastic flow and fracture.

Preferred Orientation

Preferred orientation or "texture" is recognized as an important factor affecting the final properties of cold worked materials. Since many properties of a crystal depend on the direction they are measured, it follows that a polycrystalline material will reflect this dependence on direction if texture is present. Rosenfield[33] shows that the yield strength, ductility and work hardening characteristics of face-centered cubic single crystals are markedly affected by direction. When the <111> direction is parallel to the wire axis the yield strength will be higher, the ductility will be less and the rate of work hardening will be greater than when the <001> texture is predominate. Rosenfield[33] and Bonefacic et al[34] report that wire drawing produces a texture having <111> as the major component and <001> as a minor component in face-centered cubic metals. In conventional extrusion of aluminum Takahashi and Kobayashi[35] and Bonefacic et al[34] report that the <111> fibre texture predominates, but the percentages

of <111> versus <001> may be varied by the temperature of the billet, die angle and composition of the alloy. Rosenfield shows that the most important factor influencing texture is the preformed texture, i.e., if <001>predominates before working it will predominate after working also. Vandermeer and McHargue[36], however, report that when aluminum with an initial <111> texture is conventionally extruded at low temperatures (77°K), the texture after extrustion is 90% <111> and 8% <001>. Bonefacic and Takahashi agree that the percent of <001> produced increases with temperature up to 500°C, although the amount of increase is in question. This may be explained by the fact that Bonefacic also shows that the percent of <001> also increases with increasing purity of the aluminum and the composition of Takahashi's samples is not known.

Takahashi and Bonefacic disagree on the influence of die angle on the final texture, Takahashi reporting that an increase in die angle increases the percent of <001> while Bonefacic shows that the percent of <001> decreases with increasing die angle. This discrepancy may be explained by the difference in temperature at which the die angle tests were conducted.

The temperature dependence of texture may be related to the yield and tensile strength data obtained by Hero and Mikkelsen[37] and Lengyel and Culver[38]. These studies involving the hydrostatic extrusion of aluminum into atmospheric pressure showed that the yield strength increased to a maximum with increasing extrusion

ratio and then decreased. This was attributed to dynamic recovery produced at the higher temperatures encountered at high reductions and may be related to the change in predominate texture reported by Bonefacic and Takahashi.

Dislocations

The effect of hydrostatic pressure on dislocations has been reported by several investigators. Inoue and Nishihara[39] report that the application of a high hydrostatic pressure to polycrystalline zinc results in the movement of dislocations to the grain boundaries, resulting in the buildup of dislocation walls and a subsequent strengthening of the zinc. Hanafee and Radcliffe[40] show that the application of hydrostatic pressure substantially decreases the dislocation velocity at a given stress in Lithium Flouride single crystals with and without impurities. Pines and Syrenko[41] state that although the movement of dislocations is slowed by pressure the stability of dislocations is diminished under pressure due to the volume increase required by the formation of a dislocation. Their studies of annealing aluminum under high pressure show that the dislocation density decreases with increasing pressure.

Considerable work has been performed concerning the effect of grain size on flow strength. Zhurkov et al[42] and Hero and Mikkelsen[37] are in agreement that the most important factor affecting flow stress is the arrangement of dislocations in the cell walls, i.e., the degree of mosaic block disorientation as affected by the density of dislocations in the boundaries, and not the cell or grain size.

BIBLIOGRAPHY

1. von Mises, R., "Mechanik der festen Körper in plastisch deformablem Zustand", Goettinger Nachr., Math. - Phys. kl. pp. 582-592, (1913).

2. Thomsen, E. G., C. T. Yang, S. Kobayashi, Mechanics of Plastic Deformation in Metal Processing, Macmillan Co., New York, N. Y., p. 92, (1965).

3. Bridgman, P. W., "Fracture and Hydrostatic Pressure", American Society for Metals, pp. 246-261, (1948).

4. Bridgman, P. W., "Effects of High Hydrostatic Pressure on the Plastic Properties of Metals", Review of Modern Physics, 17, pp. 3-14, (1945).

5. Beresnev, B. I., D. K. Bulychev, M. G. Gaydukov, Ye. D. Martynov, K. P. Rodionov and Yu. N. Ryabinin, "Closing of Pores and Cracks in Copper due to High Pressure Hydroextrusion", Fiz. Metal. Metalloved, 18, pp. 778-783, (1964).

6. Avitzur, Betzalel, A Survey of the Study of Flow through Conical Converging Dies, published by Dept. of Metallurgy and Materials Science, Lehigh Univ., Bethlehem, Penna., pp. 21-24, (1968).

7. Coffin, L. F. and H. C. Rogers, "Influence of Pressure on the Structural Damage in Metal Forming Processes", Transactions of the ASM, 6D, pp. 672-686, (1967).

8. Gelles, S. H., "Hydrostatic Forming - A Survey", Journal of Metals, pp. 35-46, (Sept. 1967).

9. Fuchs, F. J., "Production Metal Forming with Hydrostatic Pressures", ASME Paper 65-Prod.-17.

10. "High Pressure Forming, Extrusion Break Metalworking Barriers", Steel, pp. 62-65, Nov. 15, (1965).

11. Avitzur, Betzalel, Metal Forming: Processes and Analysis, McGraw-Hill Book Co., New York, N. Y., (1968).

12. Dieter, G. E., Mechanical Metallurgy, McGraw-Hill Book Co., New York, N. Y., p. 253, (1961).

13. Wistreich, J. G., "Investigation of the Mechanics of Wire Drawing", Proc. Inst. Mech. Engrs., vol. 169, pp. 654-665, (1955).

14. Bell, G. A., "The Measurement of Small Changes in Density in Large Specimens", Australian Journal of Applied Science, 9, pp. 236-244, (1958).

15. Rogers, H. C. and L. F. Coffin, "Investigation of the Nature of Structural Damage in Metal-Forming Processes", Progress Report to Naval Air Systems Command, Contract NOw 66-0546-d, (1966).

16. Schmehl, G. L., "The Effects of Deformation Under Hydrostatic Pressure Upon the Mechanical Properties of EC Aluminum", Master of Science Thesis, Lehigh University, June 1969.

17. Ahmed, N., "On a Phenomenological Stress-Strain Relationship for the Elastic-Plastic Deformation of Aluminum and Copper", unpublished memorandum.

18. Cartwright, J. S., Western Electric Co., Engineering Research Center, Princeton, N. J., private communication.

19. Johnson, W. and H. Kudo, The Mechanics of Metal Extrusion, Manchester University Press, Manchester, (1962).

20. Avitzur, B., "Analysis of Wire Drawing and Extrusion Through Conical Dies of Large Cone Angle", Trans. ASME, Ser. B., vol. 86, pp. 305-316, (1964).

21. Streeter, V. L., editor, Handbook of Fluid Dynamics, McGraw-Hill Book Co., New York, N. Y., (1961).

22. Hsu, S. T., Engineering Heat Transfer, D. Van Nostrand Co., Princeton, N. J., (1963).

23. Kubaschewski, O., E. Ll. Evans and C. B. Alcock, Metallurgical Thermochemistry, Pergamon Press, New York, N. Y., (1967).

24. Robertson, J., Brit. Patent Spec. No. 19356, (1894).

25. Bulychev, D. K., B. I. Beresnev, M. G. Gaydukov, Ye. D. Martynov, K. P. Rodionov, and Yu. N. Ryabinin, "Possibility of Eliminating Pores and Cracks in Metals During Plastic Deformation Under High Hydrostatic Pressures", Fiz. Metal. Metalloved, 18, (3), pp. 437-464, (1964).

26. Ryabinin, Yu. N., "Effect of Pressure on the Mechanical Properties of Solids", Journal of Chemistry and Physics, 63, pp. 1092-1095, (1967).

27. Pugh, H. Ll. D., "Recent Developments in Cold Forming", Bulleid Memorial Lectures, Vol. III B, pp. (4)33-(4)36, (1965).

28. Pugh, H. Ll. D., "The Mechanical Properties and Deformation Characteristics of Metals and Alloys Under Pressure", Int. Conf. on Materials, (American Soc. Test. Mater.), (1964).

29. Avitzur, B., "Analysis of Central Bursting Defects in Extrusion and Wire Drawing", Journal of Eng'g. for Industry, Trans. ASME, (1968).

30. Uy, J. C., C. J. Nolan and L. E. Davidson, "The Hydrostatic Extrusion of Nickel-Base Superalloys at Room Temperature", Transactions of the ASM, 60, pp. 693-698, (1967).

31. Bobrowsky, A., E. A. Stack, A. Austen, "Extrusion and Drawing Using High Pressure Hydraulics", ASTME Paper No. SP65-33, (1965).

32. Austen, A. R.,Kaklow, K. J. and E. Rozovsky, Hydrostatic Extrusion of High Strength Steel, Lehigh University Institute of Research, (April, 1968).

33. Rosenfield, A. R., "Development of Preferred Orientations", Metal Deformation Processing, Vol. I, DMIC Report 208, Battelle Memorial Institute, (1964).

34. Bonefacic, A. D. Kunstelj, M. Stubicar, and A. Tonejc, "Dependence of Texture on Processing Conditions in Extruded Aluminum Wires", Trans. of the Metallurgical Society of AIME, 242, (7), pp. 1461, (1968).

35. Takahashi, T. and Y. Kobayashi, "On the Texture of Aluminum Rods Extruded Under Various Conditions", Japan Inst. Light Metals, 18, (2), pp. 81-87, (1968).

36. Vandermeer, R. A. and C. J. McHargue, "The Nature of the Fibre-Texture Component in Extruded Aluminum Rod", Trans. of the Metallurgical Society of AIME, 230, pp. 667-675, (1964).

37. Hero, H. and J. A. Mikkelsen, "Some Mechanical and Structural Properties of Hydrostatically Extruded Aluminum and Aluminum Alloys", Journal of the Institute of Metals, 97, pp. 18-22, (1969).

38. Lengyel, B. and L. E. Culver, "Properties of Materials Extruded by Orthodox Hydrostatic Extrusion", Journal of the Institute of Metals, 97, pp. 97-103, (1969).

39. Inoue, N. and M. Nishihara, "A Strengthening Effect of High Hydrostatic Pressure Grain Boundary Walls of a Polycrystalline Zinc", Nature, 207, pp. 1188-1189, (1965).

40. Hanafee, J. E. and S. V. Radcliffe, "Effect of Hydrostatic Pressure on Dislocation Mobility in Lithium Fluoride", Journal of Applied Physics, 38, (11), pp. 4284-4294, (1967).

41. Pines, B. Ya. and A. F. Syrenko, "Change in Dislocation Density in Aluminum and Lithium Fluoride After Annealing Near the Melting Point Under Hydrostatic Pressure", Journal of Materials Science, 3, pp. 80-88, (1968).

42. Zhurkov, S. N., V. I. Betekhtin and A. I. Petrov, "Relation of the Strength of Metals with Mosaic Block Disorientation and Crystallite Size", Fiz. Metal. Metalloved., 23, (6), pp. 1101-1107, (1967).

VITA

J. Edward Oldis was born on August 13, 1933 in Trenton, New Jersey. He attended elementary school and high school in Pennington, New Jersey, from which he graduated in 1951.

He then attended General Motors Institute, Flint, Michigan as a cooperative engineering student sponsored by the Ternstedt Division, Trenton, New Jersey Plant. He graduated in 1956 with the degree of Bachelor of Mechanical Engineering.

He was then employed by the Ternstedt Division, G.M.C. in Trenton, New Jersey and subsequently by the Boeing Company, Seattle, Washington.

In 1960 he joined the Western Electric Company as a planning engineer and simultaneously attended evening school at Stevens Institute of Technology, Hoboken, New Jersey, where he received the degree of Master of Science in June, 1964.

In June, 1968 he entered the Graduate School of Lehigh University as a member of the Western Electric-Lehigh University Fellowship Program, while employed at the Western Electric Company Engineering Research Center, Princeton, New Jersey.